Nederlandse Organisatie voor
toegepast-natuurwetenschappelijk
onderzoek / Netherlands Organisation
for Applied Scientific Research

TNO Defence, Security and Safety

ONGERUBRICEERD

TNO Defence, Security and Safety
Oude Waalsdorperweg 63
P.O. Box 96864
2509 JG The Hague

www.tno.nl

T +31 70 374 00 00
F +31 70 328 09 61
Info-DenV@tno.nl

TNO report

TNO-DV1 2005 A004

Analysis of an emitter location algorithm for use in ESM systems

Date	September 2005
Author(s)	Drs. J.S. Groot
Classification report	Ongerubriceerd
Classified by	LtKol J.P. Strijker
Classification date	
Title	Ongerubriceerd
Managementuittreksel	Ongerubriceerd
Abstract	-
Report text	Ongerubriceerd
Appendices	Ongerubriceerd
Copy no	5
No. of copies	13
Number of pages	44 (incl. appendices, excl. RDP & distributionlist)
Number of appendices	1

DISTRIBUTION STATEMENT A
Approved for Public Release
Distribution Unlimited

The classification designation Ongerubriceerd is equivalent to Unclassified, Stg. Confidentieel is equivalent to Confidential and Stg. Geheim is equivalent to Secret.

All rights reserved. No part of this report may be reproduced in any form by print, photoprint, microfilm or any other means without the previous written permission from TNO.
All information which is classified according to Dutch regulations shall be treated by the recipient in the same way as classified information of corresponding value in his own country. No part of this information will be disclosed to any third party.
In case this report was drafted on instructions from the Ministry of Defence the rights and obligations of the principal and TNO are subject to the standard conditions for research and development instructions, established by the Ministry of Defence and TNO, if these conditions are declared applicable, or the relevant agreement concluded between the contracting parties.
© 2005 TNO

AQ F06-11-7955

Analysis of an emitter location algorithm for use in ESM systems

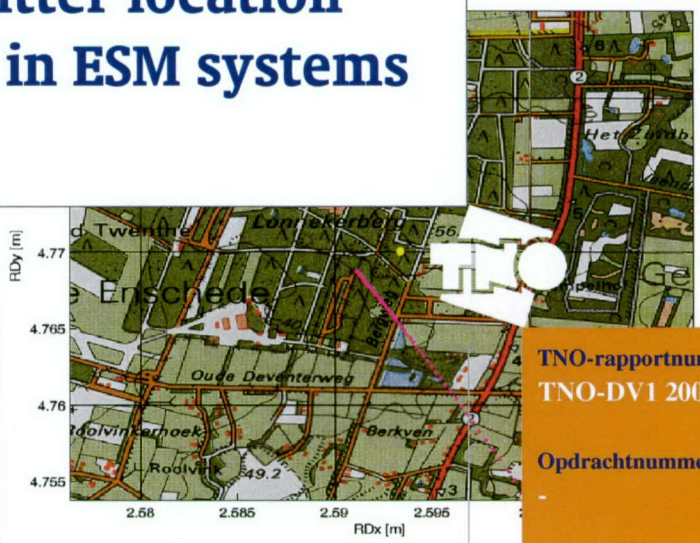

TNO-rapportnummer
TNO-DV1 2005 A004

Opdrachtnummer
-

Datum
September 2005

Auteur(s)
Drs. J.S. Groot

Rubricering rapport
Ongerubriceerd

Probleemstelling

De Klu heeft belang bij het bepalen van de locatie van radar- en communicatiezenders vanuit een vliegend platform. Als onderdeel van een ESM ("Electronic warfare Support Measures") systeem kan vanuit een vliegtuig een tijdreeks van frequenties (inclusief de Doppler verschuiving) van een zender gemeten worden. Met een dergelijke tijdreeks in combinatie met vliegtuigpositie- en snelheidsmetingen kunnen zenderlocaties benaderd worden. Daarvoor zijn diverse algoritmes beschikbaar, waarvan er één op nauwkeurigheid onderzocht is in dit project. De resultaten van dit onderzoek geven inzicht in de te verwachten nauwkeurigheid van emitter plaatsbepaling voor toekomstige ESM systemen.

Beschrijving van de werkzaamheden

De bruikbaarheid is onderzocht van een kleinste-kwadraten algoritme dat de positie en zendfrequentie van een zender bepaalt uit een tijdreeks van frequentiemetingen en vliegtuigbaanmetingen. De fout van dit algoritme is gelijk aan de "Cramér-Rao bound" en daardoor is er geen soortgelijk algoritme dat beter presteert. Voor verschillende varianten van het algoritme zijn analytisch resultaten afgeleid. Daarnaast zijn er door Monte Carlo simulatie resultaten verkregen.

Resultaten en conclusies

De positienauwkeurigheid verbetert naarmate de frequentie- en snelheidsfouten afnemen. Een hoge zendfrequentie en een vaak uitgevoerde frequentiemeting zijn ook voordelig. Meestal zullen de meettijd en de vliegsnelheid ook zo hoog mogelijk moeten zijn. De vlieghoogte is minder belangrijk. Een 2D variant van het algoritme (die de hoogte van de zender niet schat) geeft een horizontale fout door de hoogte van de zender. Bij een hoogte van 10 meter bedraagt deze fout in 2 % van een aantal gesimuleerde gevallen meer dan 100 meter. Dus als een hoge positienauwkeurigheid van belang is, dan is de 2D variant alleen in vlakke gebieden te gebruiken en kan in de andere gebieden beter de 3D variant gebruikt worden.
In 2004/2005 worden vanuit een Fokker 60 aan een Raytheon ASR-10SS radar ("Air Surveillance Radar") metingen uitgevoerd, de zgn. PESMO ("Precisie ESM Ontvanger technologie") metingen. Het 3D algoritme geeft hiermee naar verwachting een nauwkeurigheid van ongeveer 30 meter (bij 5 kilometer afstand) tot 30 kilometer (200 kilometer afstand), bij 100 seconden meettijd. Bij minder dan 25 seconden meettijd volgen geen bruikbare resultaten, doordat het aantal metingen nauwelijks het aantal te schatten parameters overtreft.
De nauwkeurigheid is afhankelijk van de afstand, en is goed genoeg om een "targeting pod" met een openingshoek van 2 graden in een tientallen kilometers groot gebied te sturen. Een (bijna) rechte baan geeft slechte resultaten.

Toepasbaarheid

Er zijn nu diverse varianten van het algoritme beschikbaar voor verwerking van de PESMO data. Met de resultaten kunnen meetscenario's bepaald worden waarmee optimale lokalisatienauwkeurigheid verkregen wordt.

ONGERUBRICEERD

TNO Defensie en Veiligheid

Lange Kleiweg 137
2288 GJ Rijswijk
Postbus 45
2280 AA Rijswijk

www.tno.nl

T 015 284 30 00
F 015 284 39 91
E info-DenV@tno.nl

PROGRAMMA	**PROJECT**
Programmabegeleider LtKol. J.P. Strijker, CTL/AJO/HSEOV	Projectbegeleider LtKol. J.P. Strijker, CTL/AJO/HSEOV
Programmaleider Dr.ir H.M.A. Schleijpen, TNO Defensie en Veiligheid	Projectleider Ir. F.A.M. Dam, TNO Defensie en Veiligheid
Programmatitel EOV-KLu	Projecttitel Emitter Lokalisatie
Programmanummer V408	Projectnummer 015.34097
Programmaplanning Start 1-1-2004 Gereed 31-12-2007	Projectplanning Start 1-1-2004 Gereed 31-12-2007
Frequentie van overleg Met de programma/projectbegeleider werd 2 maal gesproken over de invulling en de voortgang van het onderzoek.	Projectteam Ir. F.A.M. Dam Drs. J.S. Groot Ir. A. Theil

ONGERUBRICEERD

Contents

1 Introduction

The Royal Netherlands Air Force uses locations of transmitters. Part of an ESM system ("Electronic warfare Support Measures") usually consists of a capability to estimate emitter locations. This can be done from aircraft that measure a time series of transmitter frequencies (including the Doppler shift due to the aircraft motion). Beside these frequencies, estimates of the corresponding aircraft positions and velocities are needed. Several algorithms exist of which the location accuracy of one, a least-squares algorithm, had to be estimated.

Chapter 2 introduces the method and presents an example result of the iterative algorithm.

Chapter 3 introduces the Cramér-Rao lower bound (CRLB). This bound is the average minimum location error one can expect from the particular data and parameters input to *any* (unbiased) location algorithm. For five parameters an analytical relation for the error is derived. These relations are validated in Chapter 5 by Monte Carlo simulation. For the remaining parameters, for which no analytical relation could be derived, similar simulations were performed to get a feel for their impact on the location error (Chapter 6).

The algorithm in its original form estimates the x-, y- and z-coordinates of the emitter along with the emitter frequency. The Netherlands is a fairly flat country with altitude variations less than 330 m, so emitter altitude information in this area is not always needed. In Chapter 7 we investigate the pros and cons of *not* estimating the z-coordinate.

In 2004/2005 flights with receiving equipment on board a Fokker F60 aircraft were carried out. Chapter 8 gives expectations for the location accuracy for different flight scenarios. It also includes targeting pod computations, and straight trajectory computations.

Chapter 9 draws the main conclusions following from this research.

2 An emitter location method based on frequency measurements

Several methods exist to locate an emitter with a sequence of frequency measurements done from an aircraft [Dam, 2005]. This report is devoted to the analysis of a least-squares based method. The purpose of this section is to introduce the method.

The algorithm is outlined in Figure 2.1. Details are provided by [Fowler, 2001 and 2002]. Input to the algorithm are frequency measurements, which include a Doppler shift due to the aircraft movement. Secondly, the aircraft position and velocity are provided as measured at the time of each frequency measurement.

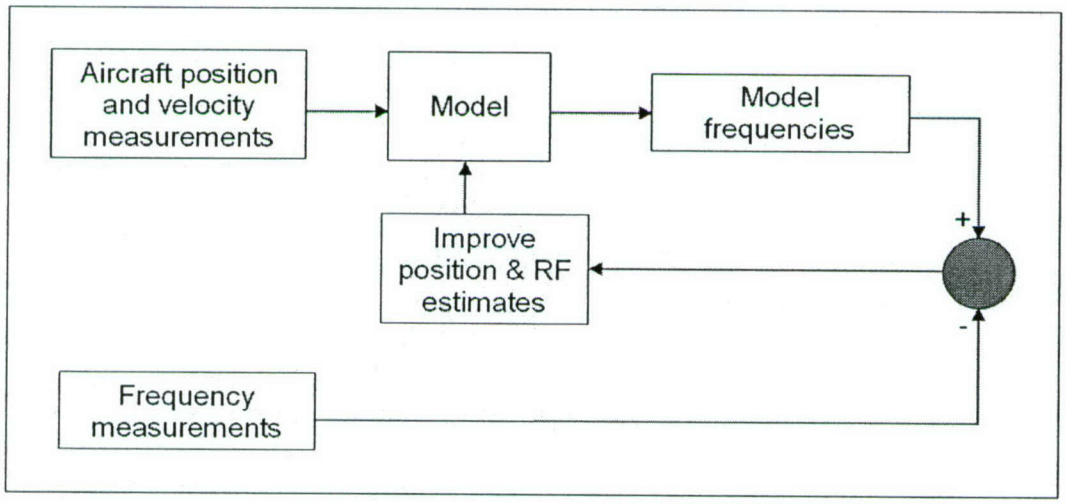

Figure 2.1: Flow diagram for the least-squares emitter location algorithm.

Assume an emitter with frequency f_0 to be at position $(x_e\ y_e\ z_e)$. We define the four-dimensional vector $\mathbf{x}(t)= (x_e\ y_e\ z_e\ f_0)^T$. The frequency of the signal as measured with a receiver from an emitter with frequency f_0 (the RF= "Radio Frequency") is now[1]

$$\tilde{f}(t) = f(t,\mathbf{x}) + \nu(t) = f_0 - \frac{f_0}{c}\,\mathbf{v}(t)\cdot\mathbf{u}(t) + \nu(t)\,. \qquad (2.1)$$

$f(t,\mathbf{x})$ is the model of Figure 2.1. The measured frequency is the emitter frequency minus a small term, the Doppler frequency shift, plus measurement noise $\nu(t)$. The Doppler frequency depends on the line-of-sight component of the aircraft velocity $\mathbf{v}(t)$, which results from the vector dot-product of the velocity with $\mathbf{u}(t)$, the unit vector pointing from the emitter to the receiver.
The algorithm calculates the model frequencies from the current estimate of the emitter location and the aircraft position and velocity. It then tries to improve the location and RF estimate by altering these such that the expected frequencies are closer to the measured ones. This is an iterative process. In fact, it is a non-linear four-parameter minimisation problem that is solved in this report with the standard iterative Gauss-

[1] In practice the signal RF frequency is mixed down to one at an intermediate frequency (IF). This lower frequency signal is what is measured. This is not important for the discussion. Therefore, we assume that the RF signal itself is measured in what follows.

Newton method. The figure below illustrates the nature of the method using simulated results. In this example the emitter location is (x_e y_e z_e)= (20000 20000 10) m and the emitter frequency f_0= 2.8 GHz.

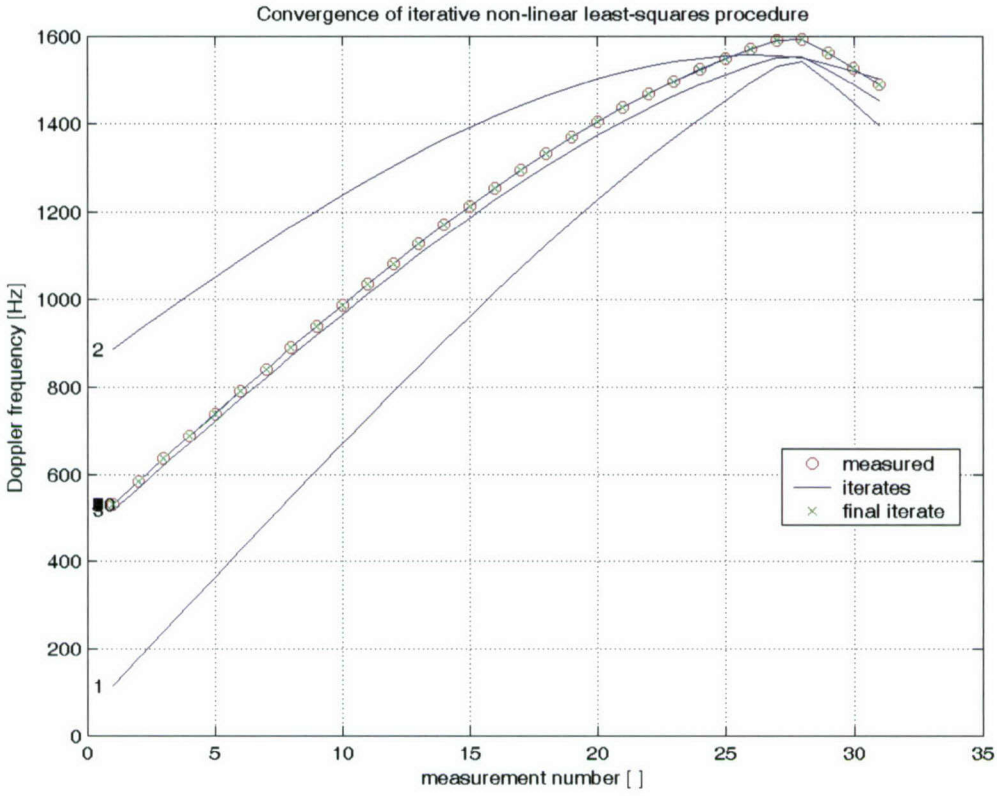

Figure 2.2: Doppler frequency versus measurement number.

The circles represent 31 Doppler measurements. These are the measured frequencies minus the emitter frequency, which is known in the simulation. The curve labelled 1 shows the computed Doppler frequency after 1 iteration of the iterative method, the one labelled 2 after 2 iterations, etc. The curves of iteration 4-10 virtually coincide (like the labels do). The crosses are the results after 10 iterations. The curves follow from an estimated emitter location and emitter frequency. The next table shows the initial values of these estimates and the values after iterations 1 to 5.

Table 2.1: Iteration results.

iteration	f-f_0 **[Hz]**	x **[m]**	y **[m]**	z **[m]**
initial values	100	24115	42527	5
1	55	21373	15982	-3893
2	-35	19629	19240	-105
3	-4	19926	19816	87
4	0	20001	20002	9
5	0	20000	20000	10

It is clear that the values converge quickly, just like the curves in the figure converge to the measurements and eventually coincide. After iteration 5 no changes larger than 1 Hz and 1 m occur.

3 Theory

3.1 Introduction

The location error (in x, y and z) of the method outlined in the previous chapter is zero when no noise of any kind is present. In practical situations noise is present and the error is non-zero, and depends on the input parameters. For example, when more frequency measurements are available one can expect a better accuracy.

When the estimation method is *unbiased* (as the method above is) the accuracy never exceeds the Cramér-Rao lower bound (CRLB). This bound depends on the particulars of the input data, which are contained in the Jacobian **H** and the data covariance matrix **C**. It does *not* depend on whatever method is used to estimate the location (but it is restricted to unbiased methods). The computation of the CRLB is explained in the remainder of the chapter. Its purpose is to predict the performance of the algorithm, which is done in the chapters to follow.

3.2 The Jacobian

The Jacobian is derived from the function $f(t, \mathbf{x})$ of Eq.(2.1):

$$f(t,\mathbf{x}) = f_0 - \frac{f_0}{c}\,\mathbf{v}(t)\cdot\mathbf{u}(t)\,.$$

The Jacobian **H** consists of four column vectors. The column vectors result from:

1 Partial differentiation of this function with respect to u_x, u_y, u_z and f_0 (for the four columns from left to right). For example, differentiation with respect to u_x gives the leftmost column

$$H_1 = \frac{f_0}{c}\left[\frac{v_x}{r} - \frac{u_x\,\mathbf{v}\cdot\mathbf{u}}{r^3}\right]. \qquad (3.1)$$

2 Substituting the measured aircraft positions and velocities, and an assumed emitter location and frequency into the result, for all N frequency measurements.

The resulting Jacobian is an $N\times4$ matrix. [Fowler, 2002] contains the complete equations. The rightmost (frequency) column consists of numbers that are close to 1. Because four parameters have to be estimated at least four frequency measurements must be performed.

3.3 The covariance matrix

The covariance matrix **C** is diagonal if we assume zero correlation between the measurement errors. In that case it can be written as

$$\mathbf{C} = \sigma_f^2\mathbf{I}\,, \qquad (3.2)$$

with **I** the $N \times N$ identity matrix and σ_f the frequency error in Hz. This error is the standard deviation of a zero-mean Gaussian distribution. It accounts for the limited accuracy of the frequency measurements.

3.4 The Cramér-Rao lower bound

The CRLB follows from the Fisher information matrix (FIM) defined by

$$\mathbf{J} = \mathbf{H}^T\mathbf{C}^{-1}\mathbf{H}. \tag{3.3}$$

H is an $N \times 4$ matrix and **C** an $N \times N$ matrix, with N the number of frequency measurements. Hence the FIM is a 4×4 matrix. The 4 follows from the fact that not only the three emitter location co-ordinates (x_0, y_0, z_0) are estimated but also f_0. This frequency is in fact a nuisance parameter, because our primary interest lies with the three co-ordinates.
In order to visualise the four-dimensional error ellipsoid we project it onto a plane formed by two of the parameters, usually the x-y plane. This particular projection is accomplished by

$$\mathbf{J}_{\text{proj}} = [\mathbf{P}\,\mathbf{J}^{-1}\mathbf{P}^T]^{-1}, \tag{3.4}$$

with $\mathbf{P} = \begin{bmatrix} 1 & 0 & 0 & 0 \\ 0 & 1 & 0 & 0 \end{bmatrix}$.

P has ones in the positions of the parameters that form the plane. The lengths of the two ellipse axes are twice the square roots of the two reciprocal eigenvalues of $\mathbf{J}_{\text{proj}}$ (a 2×2 matrix). On average, 39 % of the measurements fall inside the ellipse.

Figure 3.1 gives an example of CRLB ellipses for a certain measurement configuration. The horizontal axis is in the x-direction, the vertical one in the y-direction. The aircraft follows a weaving track along the x-axis, starting at (0,0). CRLB ellipses are plotted at grid points on a 10 km × 10 km grid. The ellipse sizes (drawn to scale) and directions vary from point to point. Generally, the accuracy of an emitter location estimate improves as the range decreases.

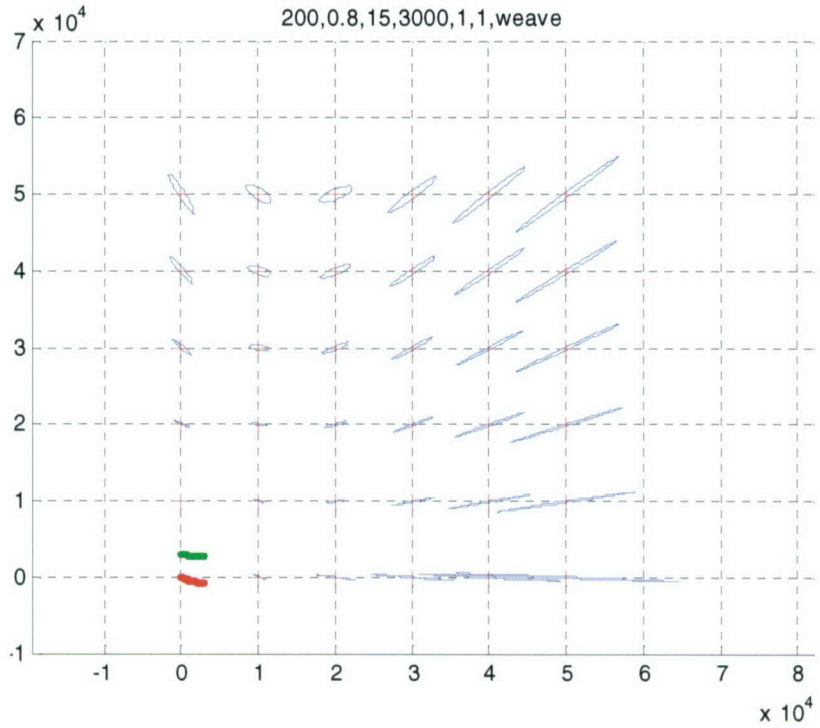

Figure 3.1: Example CRLB ellipse after [Dam, 2005]. Horizontally x [m], vertically y [m]. The weaving segments near (0,0) are top- (red) and side (green) views of the track.

3.5 Location error dependencies

From the way a CRLB ellipse is computed it follows that the location error depends on the:

1 Frequency error σ_f.
2 Aircraft velocity error σ_v.
3 Aircraft position error σ_p .
4 Emitter frequency f_0.
5 Time interval between frequency measurements dt.
6 Observation period T.
7 Aircraft altitude z_a.
8 Aircraft track (e.g., circle radius r).
9 Aircraft speed v_a.
10 Emitter location (x_e, y_e), or distance $r_e = \sqrt{x_e^2 + y_e^2}$.
11 Emitter altitude z_e.

The aircraft track and speed errors are present because the track and speed are always measured with limited accuracy. The number of frequency measurements is $N \approx T/dt$.

The dependence on parameters 1 to 5 is derived analytically in Chapter 4. The others are investigated by Monte Carlo simulation only, in Chapter 6. This kind of simulation is also used to check the analytical results in Chapter 5.

4 Location error dependencies - analytical relations

In this chapter we derive analytical relations for the dependence of the location error on five input parameters. It is done by analysing the CRLB ellipse size.

4.1 Frequency error σ_f

A frequency error σ_f due to noise influences the size of the error ellipse. We show that the size is linearly proportional to this error. Substituting Eqs.(3.2) and (3.4) in Eq.(3.3) leads to

$$\mathbf{J}_{\text{proj}} = [\mathbf{P}\,\mathbf{J}^{-1}\mathbf{P}^{\mathrm{T}}]^{-1} = [\mathbf{P}\,[\mathbf{H}^{\mathrm{T}}\,(\sigma_f^2 \times \mathbf{I})^{-1}\,\mathbf{H}]^{-1}\,\mathbf{P}^{\mathrm{T}}]^{-1} = [\mathbf{P}\,[\mathbf{H}^{\mathrm{T}}\,\mathbf{H}]^{-1}\,\mathbf{P}^{\mathrm{T}}]^{-1} / \sigma_f^2 \equiv \mathbf{K} / \sigma_f^2.$$

The eigenvalues of $\mathbf{J}_{\text{proj}}$ are $1/\sigma_f^2$ times the eigenvalues of matrix **K.** The ellipse axes are therefore linearly proportional to

$$\frac{1}{\sqrt{1/\sigma_f^2}} = \sigma_f .$$

This shows that the error ellipse size is linearly proportional to the frequency error. If the frequency error is 0 the ellipse collapses to a point: the estimated emitter location and frequency are exact in that case (if no other error sources exist).

4.2 Aircraft velocity error σ_v

The error ellipse depends also on the measurement error of the platform velocity. Assume this error is again Gaussian distributed, but this time with an error σ_v (in m/s). All three components of the velocity exhibit this error independently. If this error is small compared to the speed, it is possible to show that the radial speed error is also Gaussian distributed with standard deviation σ_v. We note that a radial speed error cannot be distinguished from a frequency error. Hence, the speed error mimics a frequency error $\Delta f = (f_0/c)\sigma_v$, due to the Doppler effect.

To get the estimation error (standard deviation) due to both the frequency and velocity error the square root of the sum of the variances has to be taken (as usual for independent errors). This leads to the result that the error ellipse size is linearly proportional to

$$\sqrt{\sigma_f^2 + \left(\frac{f_0}{c}\sigma_v\right)^2} . \qquad (4.1)$$

4.3 Aircraft position error σ_p

According to [Wu and Fowler, 2002] the influence of position errors on the Doppler frequency is at most $(2v)/R$ (usually in the order of 0.01) times the influence of speed errors[2]. This means that the Doppler error of a 1 cm position error is less than 1 % of a 1 cm/s speed error. Because the speed error is typically a few centimetres per second and

[2] It can be proven that a tighter upper limit is $\sqrt{2}v/R$.

the position error a few decimetres the latter is unimportant when compared to velocity errors.
The position error can be regarded as a scaled velocity error, so the location error is also linearly proportional to the position error σ_p.

4.4 Emitter frequency f_0

The emitter frequency f_0 influences the error ellipse, too. The ellipse size is inversely linearly proportional to f_0. This means that high emitter frequencies give smaller errors: a 10 GHz frequency emitter is located with half the spatial accuracy of a 5 GHz emitter (under equivalent conditions like the aircraft track), i.e. 100 m accuracy at 5 GHz implies 50 m accuracy at 10 GHz. This result can be proven by analysing the influence of the emitter frequency on the Jacobian **H**, and hence on the Fisher matrix and associated error ellipse.
This dependence, together with the dependence on the frequency error, shows that the CRLB is only dependent on the relative frequency error σ_f/f_0.

4.5 Sampling interval *dt*

The dependence of the position and frequency error (Cramér-Rao bound) of *dt* was first measured by simulating with a $0.8g$ aircraft weave, and varying the time interval (sample time) *dt*, while keeping the total time interval, *T*, constant. The next figure shows the result.

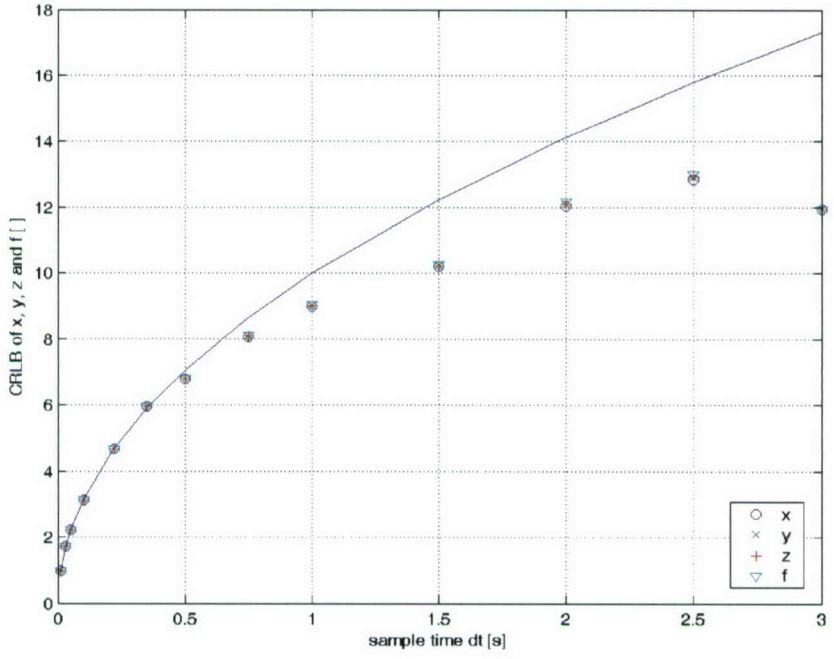

Figure 4.1: CRLB as a function of the sample time.

The CRLBs of *x* (circles), *y* (crosses), *z* (plus-signs) and *t* (triangles) are scaled by the value at the smallest sample time *dt* (= 0.01 s). Therefore, the points coincide exactly at 0.01 s. The near-coincidence of the points at all other times shows that the CRLB's differed originally only by a multiplicative factor.

The solid curve is $10\sqrt{dt}$. The measurements are close to this curve for intervals below about 0.5 s. This can be explained as follows: the error is estimated from the FIM, which depends on the Jacobian. The FIM elements are inner products of column vectors of the Jacobian. The column vectors are derivatives of functions of the platform positions and velocities. If the sample frequencies are high enough (i.e., well above the largest frequencies present in the frequency spectrum of the derivatives) the inner products increase with $1/dt$. This means that the FIM increases linearly with $1/dt$, as do the eigenvalues of the projected FIM. Consequently, the errors are linearly proportional to $\sqrt{dt}$. This explains the square root like behaviour at small dt.

Intuitively, one might expect that there would be a lower bound on the sample time below which the CRLB would not decrease any further. In reality this is not true: the plot and the derivation above show that the rate at which the error decreases increases with smaller sample times. This means that in all cases it is beneficial to measure the emitter frequency as often as possible. The reason is that the more measurements one has, the more the measurement noise is averaged out.

4.6 Conclusion

The following table summarises the dependence of the x- and y-errors on the five quantities for which analytical relations were derived. The results are also valid for the z-error because the z-direction is not fundamentally different from the x- and y-directions.

Table 4.1: Dependence of location errors on some parameters.

Quantity	**x- and y-error dependence**
Frequency error σ_f	σ_f
Aircraft velocity error σ_v	σ_v
Aircraft position error σ_p	σ_p
Emitter frequency f_0	$1/f_0$
Time interval dt	$\sqrt{dt}$ (dt< 1 s)

The dependence on a certain parameter is valid as long as the errors of the other parameters are zero. If several errors are non-zero they are combined by squaring, summing and taking the square root of the result (like what was done in Eq.(4.1)). The dependencies above are valid for arbitrary scenarios, i.e., they do not depend on particulars of the aircraft track, emitter position, etc.

5 Location error dependencies – Monte Carlo verification of analytical relations

Table 4.1 provided relations between the location error and five input parameters. We performed a Monte Carlo type simulation to check these relations.

5.1 Monte Carlo method

The simulation uses the following for the input parameters:

Table 5.1: Parameters used in the simulation.

quantity	symbol	value
frequency error	σ_f	0.1 Hz
aircraft velocity error	σ_v	0
aircraft position error	σ_p	0
emitter frequency	f_0	1 GHz
emitter co-ordinates	x_e, y_e	U(-100, +100) km
emitter altitude	z_e	U(0, 300) m
observation period	T	U(3, 60) s
sample time	dt	U(0.01, 1.00) s
aircraft altitude	z_a	U(2000, 14000) m
aircraft speed	v_a	U(80, 240) or U(-240, -80) m/s
aircraft track circle radius	r	$U(r_{min}$, 5000) m, with $r_{min} = v^2/20$ m. This limits the radial acceleration to $2g$.

$U(a, b)$ means that the values are drawn from a uniform distribution with a and b as lower and upper limit, respectively. The aircraft track was horizontal and circular[3] with its centre at (0, 0, z_a). The track starting point (on the circle) is arbitrary. In this way the emitter can be sampled during a convex as well as concave (from the emitter's viewpoint) circle segment. One should be aware of the fact that this is only one example of an infinite number of tracks.

2500 random scenarios were generated, with each scenario characterised by parameters according to (the distributions of) Table 5.1. The three-dimensional emitter position (x, y, z) and frequency were estimated with the least-squares method explained before. The next figure shows the result for the x- and y-dimension errors in the estimated emitter position.

[3] If $v_aT < 2\pi r$ the track is a circle segment, otherwise the circle is traversed more than once.

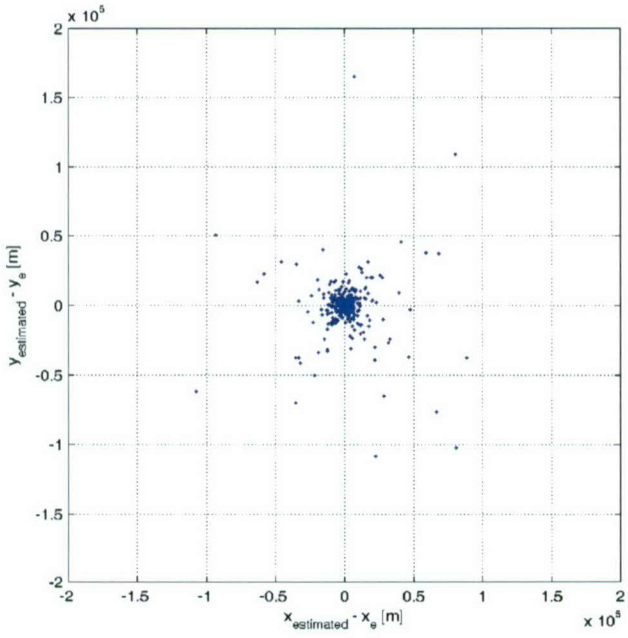

Figure 5.1: Errors in estimated emitter co-ordinates.

The averages of the location errors in x and y are near 0. The distribution is approximately circularly symmetric, as one would expect from random scenarios. r, the radial distance of the 3D points to the real 3D location of the emitter (the error distance) exhibits quite a large range. Its distribution is dominated by a large peak near 0 and exhibits a long tail. A plot of r itself is unclear and therefore we show the distribution of $^{10}\log(r)$ in Figure 5.2.

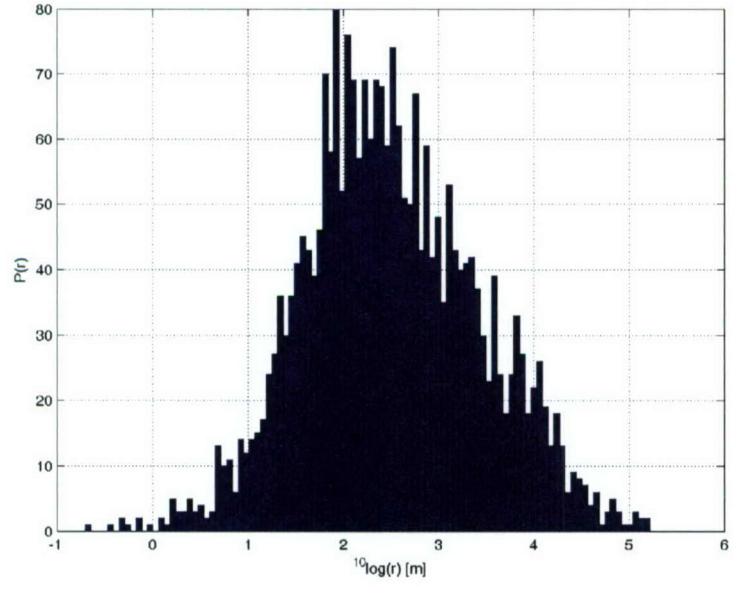

Figure 5.2: Distribution (histogram) of $^{10}\log(r)$.

The distribution resembles a slightly a-symmetric Gaussian: it extends more to the right than to the left. Had it been an exact Gaussian the distribution of r would have been

lognormal. Apparently, the *r*-distribution is even more heavy-tailed. *x* and *y* are similarly distributed.

We like to compare the results of simulations with respect to the location accuracy. The first choice for a comparison would be the standard deviation of the error distance *r*. This has a drawback. The standard deviation is by definition more sensitive to samples values far away from the mean than to nearby values. These "tail samples" of *r* occur often in the simulation, because *r* is near-lognormal distributed as was demonstrated before. The exact values of the tail samples are a matter of chance. As a consequence, the standard deviation varies much from simulation to simulation, and is a bad measure for the location accuracy. We therefore use r_{50} as a measure for the accuracy in what follows. It is defined with the help of the figure below, which shows the cumulative histogram of *r*. About 50 % of the cases exceed a radial error of 273 m, or r_{50}= 273.

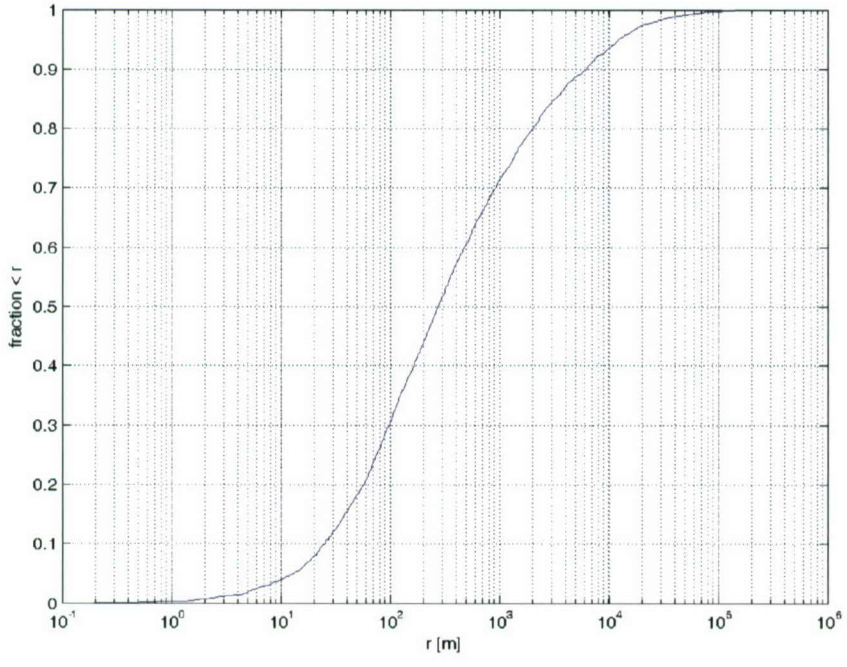

Figure 5.3: Cumulative histogram of the error distance *r*.

5.2 Algorithm stability

A complication is that the algorithm is not perfectly stable when the errors in the input data are non-zero. Two errors occur: non-convergence and an ill-conditioned Jacobian. In the example of Figure 5.1 non-convergence occurred in 3.2 % of the runs. Non-convergence means that after 20 iterations the solution had not converged. An ill-conditioned Jacobian **H** results in an inaccurate or non-existing inverse $(\mathbf{H}^T\mathbf{H})^{-1}$, which is needed in the search for the minimum. If this occurs during any of the iterations, the run is aborted. Ill-conditioning occurred in 10.0 % of the runs. In the plots above only the 2500 valid results are used.

To investigate the cause(s) of ill-conditioning we plotted the condition number (CN) as a function of the various parameters. The CN was computed as the largest singular value divided by the smallest one. When the CN is above 1/(machine precision)

problems occur. For Matlab 7.0 this means the CN should be (well) below 2^{52} for good solutions. So in the plots below ^{10}log(CN) should be below 15.6.

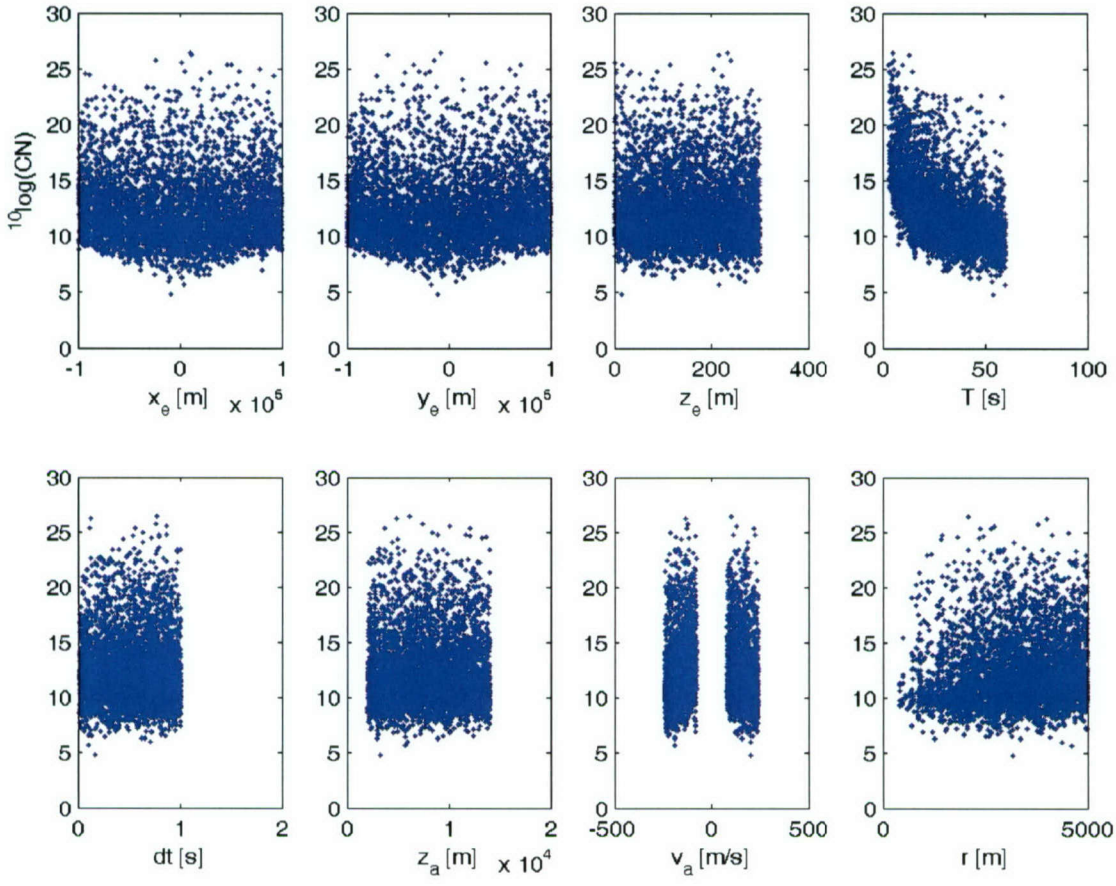

Figure 5.4: Dependence on condition number CN.

The plots show that the observation period, T, has the clearest correlation with the CN: the larger T the smaller (better) CN. This is intuitively clear: the longer one measures, the larger the probability of having obtained sufficient measurements for a reliable location determination. A less clear correlation is that smaller x_e and y_e (a smaller aircraft-emitter distance) are (on average) better, as are a larger aircraft speed, v_a, and a smaller circle radius, r. This is useful information for the implementation and use of an emitter location system based on the least-squares algorithm.
The method above is not optimal for finding correlations because many parameters are varied at the same time. A better way would be to fix only but one parameter. Nevertheless, the findings above are useful.

In the simulations above the first guesses for the location and RF were simply the exact location and RF. In practice, one does not know the exact location nor the RF. After all, these have to be estimated. One usually performs a grid search to find an initial estimate. This degrades the accuracy of the algorithm somewhat. For the simulation the grid search is too time consuming. As a substitute we spoiled the exact location and RF by a random percentage between -10 and +10 % and used this as our initial estimate.

5.3 Results

For the cases below we set T= 60 s in order to restrict our investigations to (almost only) well behaving cases, unless otherwise stated. This is also facilitated by the (unrealistically) small frequency errors. In these cases the fraction with a bad CN is less than a few percent, which also holds for the non-convergent cases (with a good CN). The table shows the result for the parameters for which we derived analytical results in the preceding chapter.

Table 5.2: Location accuracy dependence of parameters. The right column gives the quantities on which r_{50} is linearly dependent.

quantity	**values**	r_{50} **[m]**	$r_{50} \sim \ldots$
frequency error σ_f [Hz]	0.01, 0.02, 0.04	15.5, 33.6, 66.1	σ_f
aircraft velocity error σ_v [m/s][4]	0.01, 0.02, 0.04	55.3, 109, 208	σ_v
aircraft position error σ_p [m][4]	1, 2, 4	7.96, 16.4, 31.8	σ_p
emitter frequency f_0 [GHz]	1, 2, 4	155, 84.9, 39.8	$1/f_0$
sample time dt [s]	0.1, 0.2, 0.4	79.1, 115, 158	$\sqrt{dt}$

The numerical values in the table above give some credit to the derived relations which are in the right column for the standard deviation. For example, for f_0 an error ratio is 155/84.9≈ 1.8, which is close to the expected 2.
It is interesting to note that the errors due to aircraft velocity exceed those due to the position by a factor $55.3\times10^2/7.96\approx700$ (for velocity= position error). The average simulated speed is (80+240)/2= 160 m/s, and the average range follows from the bivariate uniform distribution used for the emitter location: approximately 77 km. Footnote 2 on page 12 predicts a factor of at least $77\times10^3/(\sqrt{2}\times160) \approx 340$, which is below 700 indeed.

5.4 Conclusion

The validity of the analytical relations derived in Chapter 4 is confirmed (not proven) by Monte Carlo simulation.

[4] The error was applied independently to each of the three components.

6 Location error dependencies – non-analytical relations

The preceding two chapters dealt with parameters for which analytical relations could be derived. This seems impossible for the parameters in the table below. For these we present Monte Carlo simulation results along with some discussion.

Table 6.1: Parameters used in the simulation.

name	***symbol***
observation period	T
aircraft altitude	z_a
aircraft track circle radius	r
aircraft speed	v_a
emitter co-ordinates	x_e, y_e
emitter altitude	z_e

The parameters for the simulation are those of the previous chapter, unless otherwise stated.

6.1 Observation period *T*

Figure 6.1 shows the decrease of r_{50} as the observation period increases. The circles are the simulation results; the solid line is a least-squares fit which resulted in

$$r_{50} = 28.0 + 1.90 \times 10^7 T^{-2.90}. \tag{6.1}$$

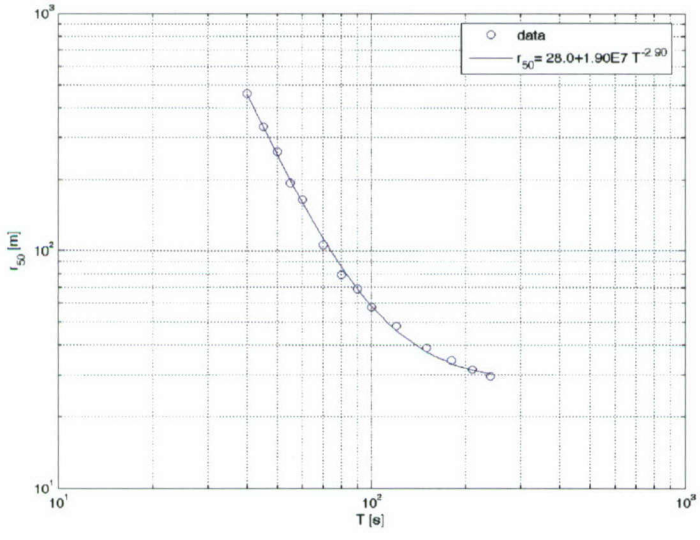

Figure 6.1: r_{50} as a function of observation period T.

The fact that a longer measurement leads to better results is not surprising. At first the improvement is rapid: almost proportional to T^{-3}. For longer times the improvement slows down. This is probably due to the fact that the longer one measures, the larger the probability that the same data is measured again: the circular track is traversed more than one time. For other track types the behaviour might be different.

6.2 Aircraft altitude z_a

The following figure shows the dependence of r_{50} on the aircraft altitude. The variation is small. Only when the altitude is below 4 km, the performance is degraded by 20 m per 1 km altitude decrease.

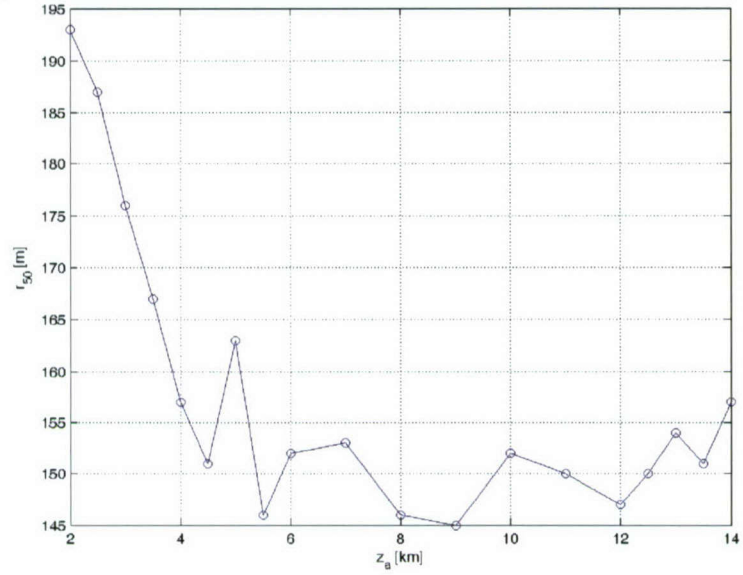

Figure 6.2: r_{50} as a function of aircraft altitude z_a.

6.3 Track radius r

r is the radius of the circular aircraft track. The function has a minimum around 1250 m. Small and especially large radii give relatively bad location accuracy.

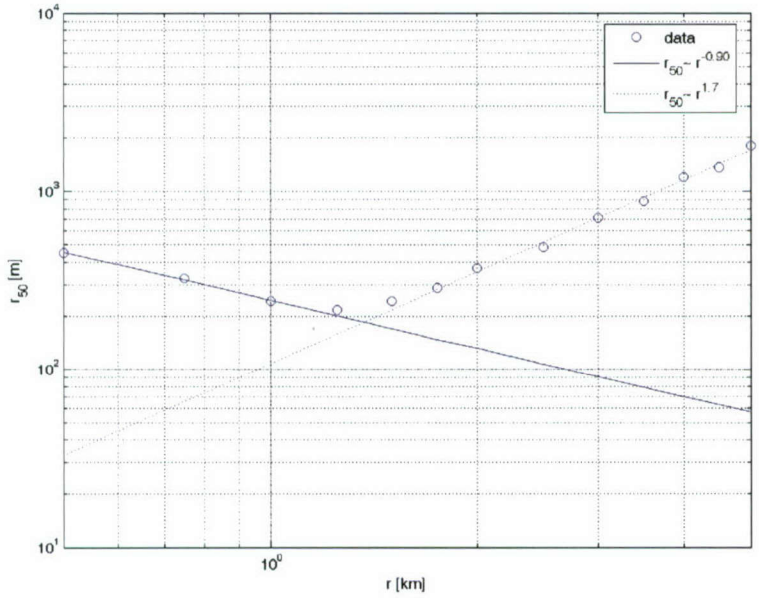

Figure 6.3: r_{50} as a function of track radius r.

Possible causes for the occurrence of a minimum are:

1 Small radii give repeated Doppler measurements (because the circle is traversed more than once), and
2 Larger radii give less useful Doppler information because the track tends to a straight-line segment (see Section 8.5).

6.4 Aircraft speed v_a

The relation between the measurement accuracy and the aircraft speed is straightforward, as shown in Figure 6.4. The measurement accuracy increases quickly with increasing aircraft speed, following a simple power law.

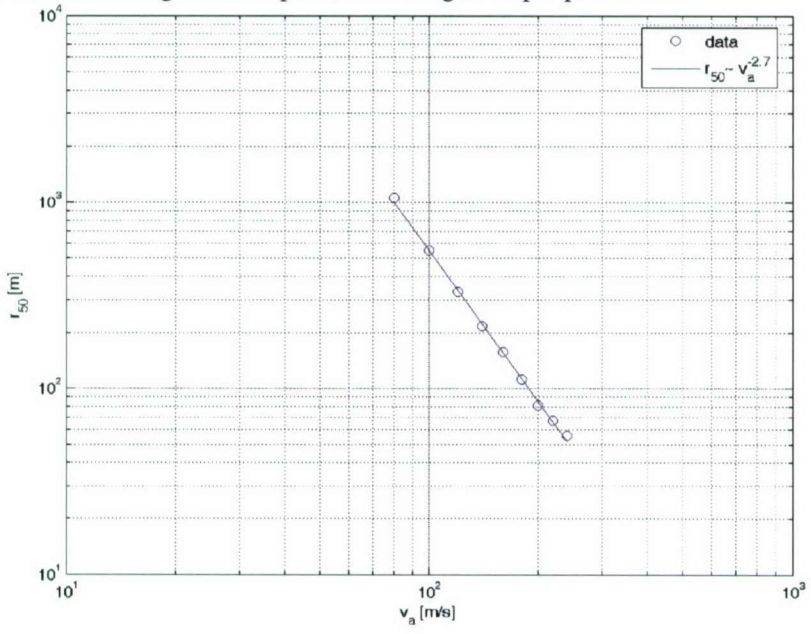

Figure 6.4: r_{50} as a function of aircraft speed v_a.

This can be made plausible by considering a measurement done at a certain speed v and a higher speed αv ($\alpha > 1$). The positions at which frequency measurements are taken are identical for the two if:

1 The time interval of the v-measurement is α times that of the αv-measurement, and
2 The observation period of the v-measurement is also α times that of the αv-measurement.

An additional effect of the higher speed is that all Doppler frequencies are higher by a factor α. The three effects together are:

1 Time interval: an accuracy decrease $\sim\sqrt{\alpha}$ (Table 4.1).
2 Observation period: an accuracy increase given by Eq.(6.1). This depends on the observation period of the αv-measurement.
3 Doppler frequency increase: an accuracy increase $\sim 1/\alpha$ (Table 4.1).

Therefore, we can compute the accuracy at speed αv from that at speed v by

$$r_{50}(\alpha v) = r_{50}(v)\frac{1}{\sqrt{\alpha}}\frac{28.0+1.90\times10^{7}(\alpha T)^{-2.90}}{28.0+1.90\times10^{7}T^{-2.90}}.$$

Inspection of this expression for different observation periods gives an approximate dependence of $\sim v_a^{-2.7}$ of Figure 6.4. However, the correspondence is certainly not perfect.

6.5 Emitter distance r_e

The emitter distance r_e is the distance between (0,0) (the center of the aircraft track projected on the earth surface) and an emitter. For various values of r_e, 2500 simulations were done with an emitter put at a random location on the circle defined by r_e. The plot of Figure 6.5 is symmetric around $r_e \approx 8$ km at which a minimum occurs. The origin of this value of 8 km is not yet clear. It is most probably an artefact of the simulation, due to the range of different altitudes and emitter distances.

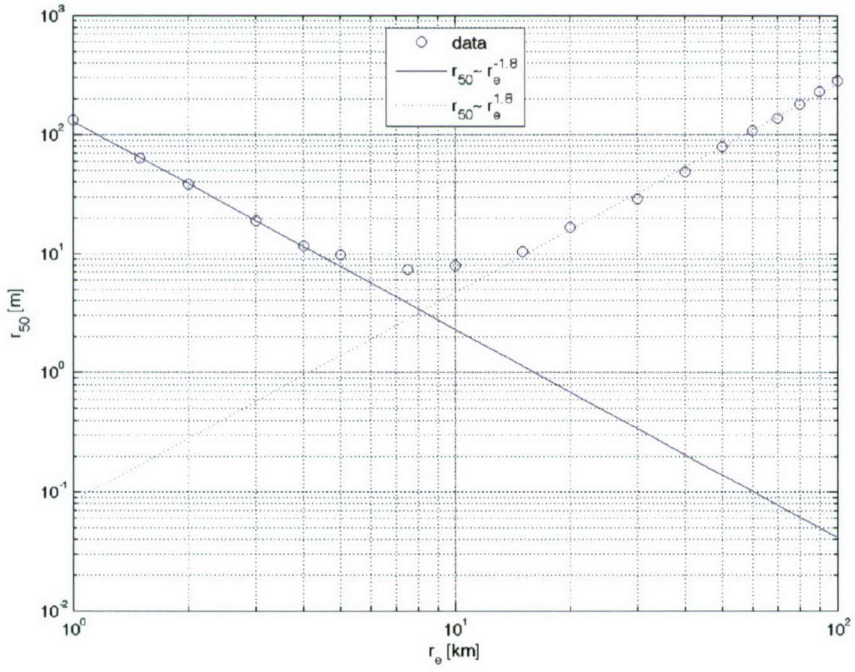

Figure 6.5: r_{50} as a function of emitter distance, r_e.

As explained in [Dam, 2005] the required location accuracy (and its dependence on emitter distance) depends on the operational use of the estimated locations. Two accuracy types can be discerned:

1 Absolute accuracy. This accuracy is expressed in meters and is essentially independent of the emitter distance. For example, if precision guided munition is used the location accuracy should be a few meters, independent of the emitter range.
2 Relative accuracy. For this accuracy the location error stays within a cone. The cone is defined by the field of view (FOV, typically 1 to 2°) of a targeting pod. Loosely speaking, relative accuracy means that the resolution does not degrade

faster than linearly with range r. However, this definition is only valid for the limit of r to infinity. Section 8.4.2 contains an example which is solved exactly.

The question whether this algorithm provides relative or absolute accuracy in the loose sense is answered by Figure 6.5: at ranges below 8 km (in this particular configuration) the algorithm provides better than absolute accuracy: its accuracy *improves* with distance instead of being constant. However, beyond 8 km range the accuracy is worse than relative accuracy (in the loose sense of above): the accuracy degrades as $r_e^{1.8}$ (as compared to r_e for relative accuracy).

6.6 Emitter altitude z_e

Figure 6.6 shows that the emitter altitude is of little significance, the curve is noise-like (note the vertical scale). This also follows from the dependence on the aircraft altitude (Figure 6.2).

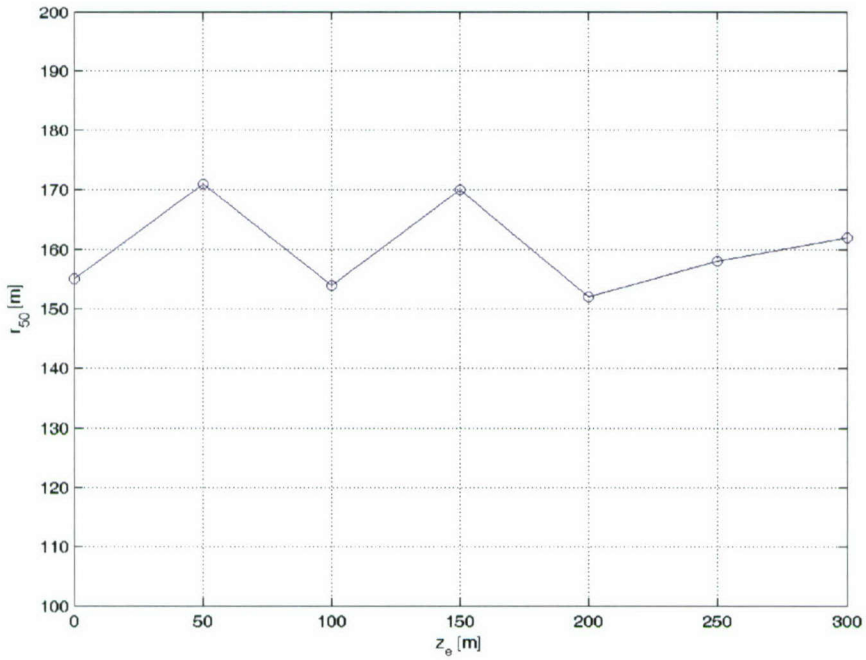

Figure 6.6: r_{50} as a function of emitter altitude, z_e. Note the vertical scale.

6.7 Conclusion

The conclusions from the simulations are:

1 The observation period T should be several tens of seconds, because the location error decreases almost with the cube of T. However, for times above about a minute this rate drops.
2 The aircraft altitude is not very important. Flying below 4 km increases the location error somewhat.
3 For circular tracks the location error is minimal for a 1250 m radius.
4 The aircraft speed should be as high as possible, because the location error decreases as $v_a^{-2.7}$.
5 The location error is smallest for emitter distances around 8 km.

6 There is no clear correlation between the location error and the emitter altitude (varied between 0 and 300 m). This holds for this three-parameter (x, y and f_0) algorithm. The next chapter discusses the four-parameter (x, y, z and f_0) algorithm.

Note that these conclusions are only valid for the general scenarios used in the preceding simulation (i.e., those described by Table 5.1). In addition, they are only valid for "the average" of these scenarios. A rough extrapolation to an arbitrary scenario is:

1 The observation period, T, should be several tens of seconds.
2 The aircraft altitude is not very important.
3 The aircraft speed should be as high as possible.
4 No clear correlation exists between the location error and the emitter altitude.

If the scenario is (partially) known a simulation should again be carried out to find the optimum measurement parameters for that particular case. This is for example done in Chapter 8 for the test flights foreseen with PESMO ("Precisie ESM Ontvanger technologie").

It should also be stressed that the above conclusions were reached for an unrealistically small frequency error of 0.1 Hz. For more realistic values (like 25 Hz in the PESMO case) the number of outliers increases and the relations above tend to be less pronounced. Relations tend to "flatten out". For example, the location error does not vary as $T^{-2.7}$ but rather as T^{-1} for a certain case.

7 Performance of the three-parameter least-squares algorithm for emitters at non-zero altitude

7.1 Introduction

The four-parameter method (denoted LSQxyz in the following) used in the previous chapters estimates four emitter parameters: the location (x, y, z) and the frequency f_0. It is easy to write a three-parameter version LSQxy which estimates (x, y) and f_0 only and assumes the emitter is at altitude z= 0 m. However, the error in x and y now depends on the real altitude of the emitter. This error should not exceed the required position accuracy. The advantages of LSQxy are faster execution and probably a more stable behaviour than LSQxyz because the search space is now three- instead of four-dimensional.
The reason to investigate LSQxy is the flat topography of The Netherlands: the lowest and highest points are at -7 m (Nieuwerkerk aan de IJssel) and +321 m (Vaalserberg, Limburg). The accuracy of LSQxy might be sufficient for this flat topography.

The results of LSQxy are compared to those of LSQxyz in section 7.2, both analytically and through simulation. The performance of LSQxy in conjunction with topographic data is investigated in section 7.3.

7.2 Comparison of LSQxy and LSQxyz results

7.2.1 Analytic approach

To gain insight in the problem we first estimate the change in Doppler frequency of an emitter at z= 0 m moved to another level h. If this change for the ≈330 m altitude variation over The Netherlands is smaller than the expected accuracy of the frequency measurements (≈25 Hz for PESMO) LSQxy's accuracy is sufficient.

According to Eq.(2.1) the (absolute) Doppler frequency is

$$f_d(h) = \frac{f_0}{c}\mathbf{v}\cdot\mathbf{u}(h)\,.$$

The Doppler frequency depends on the aircraft velocity **v** and on **u**, the unit vector pointing from the emitter to the receiver. We only showed the h-dependency. The absolute difference between the Doppler frequencies of identical emitters at altitude h and 0 is

$$\Delta f_d(h) = \frac{f_0}{c}\left|\mathbf{v}\cdot\left(\mathbf{u}(h)-\mathbf{u}(0)\right)\right|.$$

It can be shown that, if the emitter height is much less than the aircraft altitude ($h << H$), this relation holds:

$$\Delta f_d(h) < \frac{f_0 v}{2Hc}h\,.$$

It is now possible to calculate the expected difference for the PESMO test flight, for example. In that case (see sections 8.2-8.3):

- emitter frequency $f_0 \approx$ 2.9 GHz.
- aircraft speed $v \approx$ 79.8 m/s.
- aircraft altitude $H \approx$ 1524 m.
- maximum emitter altitude $h =$ 330 m (Dutch topography).

This leads to $\Delta f_d <$ 84 Hz. This upper limit exceeds the frequency accuracy of 25 Hz that we expect. This suggests that the four-parameter procedure LSQxyz should be used.

7.2.2 *Monte Carlo approach*

As shown above, Doppler frequencies occur that exceed the Doppler measurement accuracy. This suggests that LSQxy's (x, y) estimates are not accurate enough. We investigated this with the Monte Carlo simulation described in Chapter 5 with an emitter put at an altitude of 10 m. The emitter co-ordinates (and f_0) were estimated with the LSQxy algorithm for 10,000 random scenarios. We assumed that the input data (the emitter frequency, aircraft position and speed) are exact. The figure below shows the cumulative histogram of r, the radial distance of the LSQxy estimate to (0,0), i.e., the error distance.

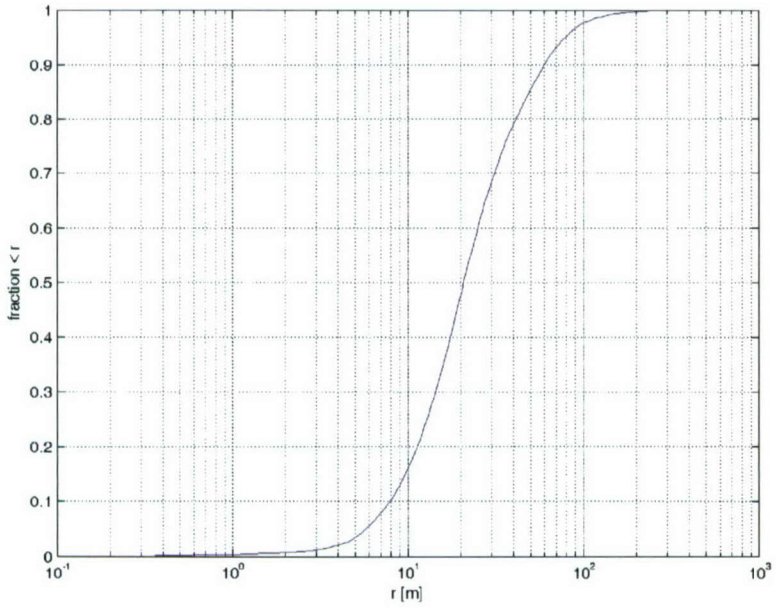

Figure 7.1: Cumulative histogram of the error distance, r.

About 84 % of the cases exceed a radial error of 10 m and 2 % exceed 100 m. A run with an emitter altitude of 100 m instead of 10 m showed that this behaviour scales linearly: 84 % of the cases exceeds a radial error of 100 m and 2 % exceeds 1000 m in this case. We conclude that the LSQxy algorithm is not accurate enough for our purposes, even for the flat Dutch topography.

7.3 Location errors of the three-parameter least-squares method incorporating topographic data

The LSQxy method estimates (x, y) and f_0. The previous section showed that neglecting the topography causes unacceptable large location errors for elevated emitters. This can be circumvented by using measured topographic data, i.e., the terrain altitude z as a function of the (x, y) position. [Fowler, 2001] shows that this influences the Jacobian only. Without the use of topography the first column (as an example) of the Jacobian is, according to Eq.(3.1):

$$\frac{f_0}{c}\left[\frac{v_x}{r} - \frac{u_x \mathbf{v}\cdot\mathbf{u}}{r^3}\right].$$

With the use of topographic data it becomes

$$\frac{f_0}{c}\left[\frac{v_x - v_z\dfrac{\partial z}{\partial x}}{r} - \frac{\left(u_x + u_z\dfrac{\partial z}{\partial x}\right)\mathbf{v}\cdot\mathbf{u}}{r^3}\right].$$

The two additional terms both include the terrain slope in the x-direction, $\dfrac{\partial z}{\partial x}$. This slope is evaluated at the current emitter location estimate.

The simulation of the previous section was repeated with the LSQxy method incorporating the modified Jacobian accounting for the topography. As an example the topography was modelled by

$$z = 5\sin(x/1000) + 150\cos(y/10000) + 2r\,.$$

r is a drawing (varying from point to point) from a Gaussian random distribution with variance 1. The altitude varies by some 310 m (mimicking the situation in The Netherlands), disregarding r. The topographic data is provided on a 100 m × 100 m grid over a 200 km × 200 km area. For non-grid points altitudes are computed by bilinear interpolation. The figure below shows the topographic map.

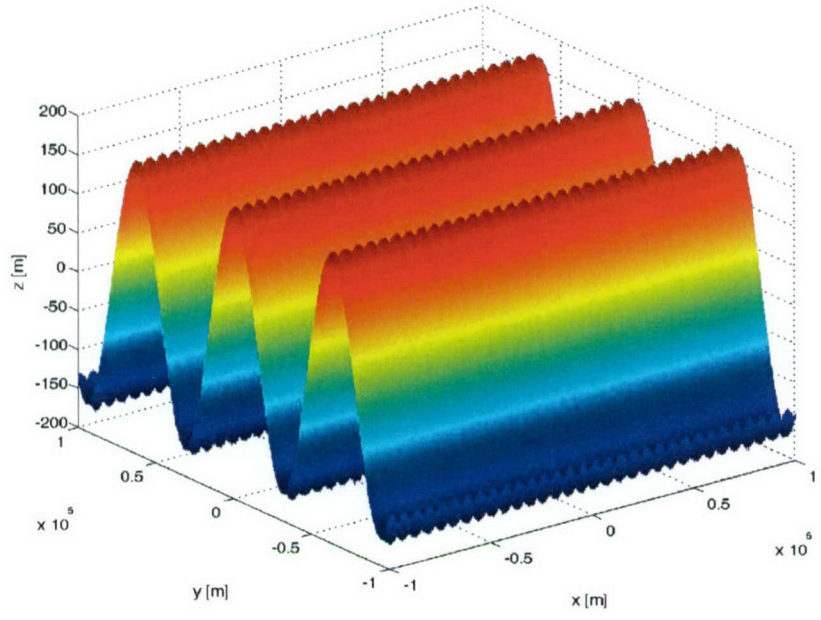

Figure 7.2: Example topographic map.

We repeated the simulation of the previous section and present the result again in a cumulative histogram of r, the error distance.

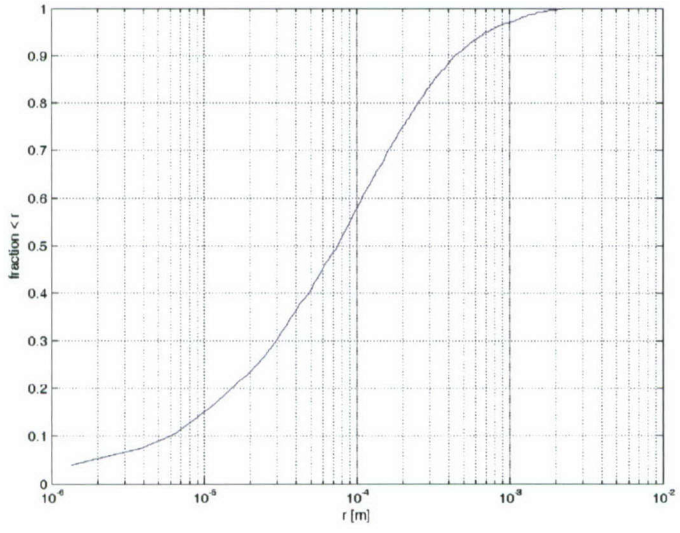

Figure 7.3: Cumulative histogram of the error distance r for the case including topographic data. Compare Figure 7.1.

All errors are well below 3 mm, which is negligible. We conclude that the LSQxy algorithm with the use of topography performs well.

7.4 Conclusion

The three-parameter algorithm LSQxy provides insufficient accuracy in the horizontal direction for emitter altitude variations of ≈330 m. This follows from both analytical considerations and Monte Carlo simulations. Used in conjunction with topographic data, the accuracy is sufficient.

8 Performance during the PESMO flight tests

8.1 Introduction

Tests with PESMO are foreseen for the end of 2004 and for 2005 [B.C.B. Vermeulen et al., 2004]. The receiving equipment is flown on board a Fokker F60 aircraft. The receiver samples the signal of the PSR ("Primary Surveillance Radar") of the Raytheon ASR-10SS ("Air Surveillance Radar"). To date, five of those radars are operated throughout The Netherlands. This chapter predicts the performance of the LSQxyz algorithm for the specific ASR waveform in combination with the flight tracks planned.

8.2 ASR waveform

The ARS repeatedly transmits a pulse sequence consisting of 40 pulses, 20 short ones and 20 long ones [Theil, 2005]. Because only the 40 long pulses are used for the frequency estimation, the short pulses are excluded from this discussion and we refer to the long ones as "pulses". Some characteristics of the 20 pulses are in Table 8.1.

Table 8.1: Pulse characteristics.

pulses	mean RF [GHz]	PRF [Hz]
1-5	2.875	1032
6-10	2.799	775
11-15	2.877	919
16-20	2.801	710

The 20 pulses are transmitted in 4 bursts of 5 pulses each. The mean RF and PRF differ per burst. The pulses exhibit non-linear frequency modulation. For our purpose the particulars of this are unimportant (details are contained in [Theil, 2005]). We simply assume that the frequency estimation algorithm provides us with an estimate of the (mean) frequency of every pulse. The expected accuracy is 25 Hz.

The ASR antenna rotates with a period of 4 s. Due to the azimuth beamwidth of 1.4° it is expected to receive about 13 pulses for every revolution. This is quite different from the scenarios discussed before in that the emitter location has to be computed now from frequency measurements that are available in an interval of ≈18 ms for only every 4 seconds.

8.3 F60 tracks

Two F60 track types are foreseen [Vermeulen et al., 2004] :

- A weaving trajectory made up of circle segments (results in section 8.4).
- A straight-line trajectory without aircraft manoeuvres (section 8.5).

For both tracks the altitude has to be below 5000 ft (1524 m), due to air traffic control regulations. The speed is kept constant at 79.8 m/s. The weave is in addition characterised by a horizontal centripetal acceleration of ±0.5g (the sign differs for

subsequent concave and convex segments) and a maximum heading deviation of ±30°, starting at -30°. The radius of the circle segments is v^2/a= 79.8/(0.5×9.81)= 1298 m. Figure 8.1 shows this weave in the upper drawing.

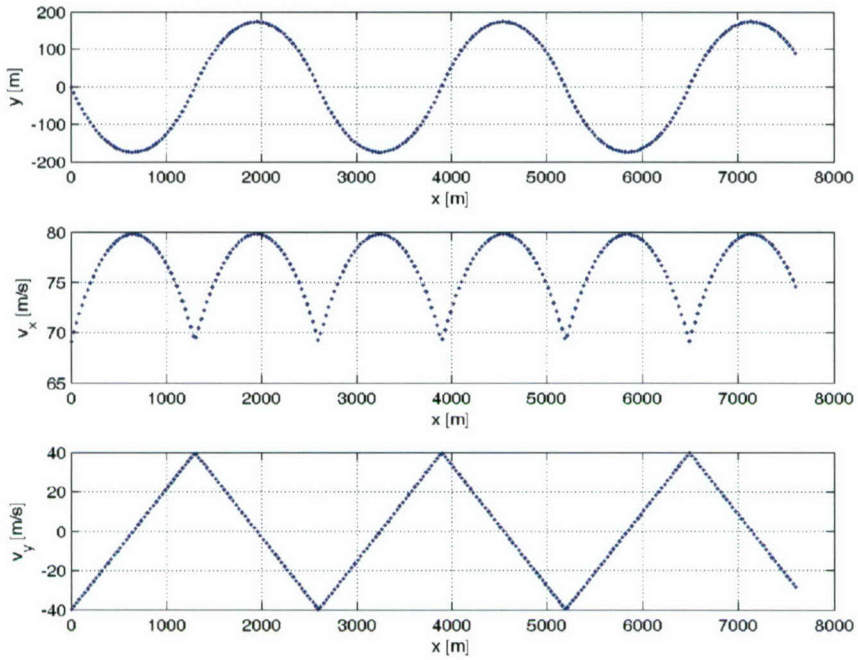

Figure 8.1: Weaving trajectory for a time span of 100 s.

The speed is the square root of the squared x- and y-components of the velocity in the two lower plots and is always 80 m/s.
Although the weave looks like a sine it really consists of circular segments. A weave resembles the practical situation in that the steering direction is periodically suddenly changed in sign by the pilot.

The dots in the plot corresponds to 0.4 s time steps, which is 1/10 of the ASR antenna revolution period. This short time step is used to visualise the weave clearly. In reality a 4 s time step (the ASR revolution period) occurs. This results in about 9 dots (= measurement intervals during which the ASR antenna beam sweeps across the aircraft antenna) per weave period. This shows that the weave period of Figure 8.1 is a reasonable choice. If the weave would last much longer, the frequency measurements would be correlated more. This happens because the aircraft is in almost the same position at consecutive ASR antenna revolutions. The correlation degrades the location estimate.

The PESMO receiver will be connected to the rear left antenna of the F60. This position is thought to be least subject to mechanical vibrations, which benefits the frequency estimation. The antenna pattern points to the rear left. The left plot of Figure 8.2 shows the rectangular area in which the emitter should be to enable the receiver to observe it for 100 s. The right plot gives the same area for 600 s.

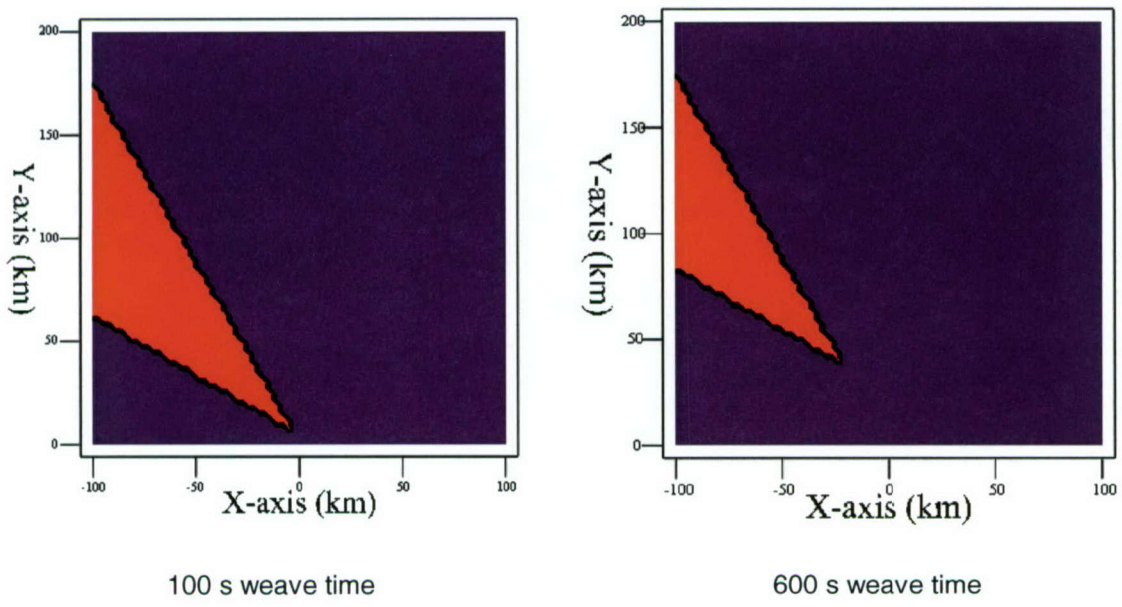

Figure 8.2: Allowed emitter positions. The track extends from (0, 0) to the right, along the positive *x*-axis.

The co-ordinates of the corners of the two triangular areas are (clockwise, starting at the lower left):

- 100 s weave time: (-100, 61), (-100, 175), (-1.4, 4.6) km
- 600 s weave time: (-100, 83), (-100, 175), (-20.0, 36.7) km

8.4 Weaving trajectory computations

8.4.1 Various scenarios

Several cases were computed with the weaving trajectory of the preceding section. The results are in Table 8.2, each row denoting a different scenario. The first six rows correspond to the corners of the triangles in Figure 8.2.

Table 8.2: Results for different scenarios. If a box is empty, the corresponding value of the basic scenario nr.1 was used.

nr.	σ_f [Hz]	σ_x [m]	σ_v [m]	x_e [km]	y_e [km]	z_e [m]	z_a [m]	v_a [m/s]	T [s]	bad CN [%]	diver-gence [%]	x_{50} [m]	y_{50} [m]	z_{50} [m]	f_{50} [Hz]
1	25	0.2	0.01	-1.4	4.6	0	1524	79.8	100	0	0	30	71	165	4.6
2				-100	61					38	25	27×10^3	16×10^3	27×10^3	14.6
3				-100	175					34	29	15×10^3	26×10^3	30×10^3	14.4
4				-20	36.7				600	8.2	38	176	306	2310	1.8
5				-100	83				600	6.6	44	2690	2283	13×10^3	4.0
6				-100	175				600	5.0	45	1364	3183	21×10^3	6.6
7	12.5									0	0	15	35	83	2.3
8			0.005							0	0	30	71	165	4.6
9							1000			0.9	4.5	29	68	212	4.2
10							5000			0	0	39	80	165	7.5
11								100		0	0	29	49	147	3.6
12									25	17	25	369	271	586	60
13	burst averaging (see text)									0	0	29	71	165	4.7
14	frequency normalisation + burst averaging (see text)									0	0	29	72	165	5.0
15	idem								25	16	25	374	268	580	62

Discussion:

1 The basic scenario, to which all the scenarios below are compared.
2 A more distant emitter increases the errors. The problem is also quite ill-conditioned.
3 See 2.
4 The 600 s of data keeps the errors within bound.
5 See 2.
6 See 2.
7 The halved frequency error approximately halves all errors, as predicted in section 4.1.
8 A smaller speed error does not lead to significantly smaller errors, as could be expected from section 4.2: the frequency error dominates the speed error. Because the speed error dominates the position error, the position error is certainly unimportant.
9 A lower aircraft altitude almost only alters the z-error somewhat. The problem starts to be ill-conditioned.
10 Some slightly larger errors.
11 An increased aircraft speed improves the position estimate a bit, but not by the amount predicted in section 6.4. This is no contradiction because that prediction was based on the average of a large number of different scenarios.
12 A shorter observation period decreases the accuracy. 25 s is the minimum time for this algorithm to produce sensible results in a reasonable time.
13 In this case the measured frequencies were averaged per burst (constant PRF and RF), as were the measured aircraft speed and position. The difference with nr. 1 is negligible. The execution speed is smaller, however. Burst averaging is therefore preferred.
14 The average of the measured frequencies of RF number 2, 3 and 4 were set equal to the average of RF number 1. It now seems like the measurements have been made

with a single RF so only this RF has to be estimated (instead of 4). The difference with scenario nr. 1 is negligible.

15 To test whether the method of nr. 14 has advantages with respect to the stability, the observation period was decreased to 25 s. The difference with nr. 12 is negligible, so (surprisingly) this method has no advantages.

The z-error exceeds in all cases the x- and y-errors, due to the constant flight level (hence no extra Doppler shift is induced by altitude variations). In practice, the flight level is rather constant, so this is to be expected in real life situations, too.

The results were computed by using all the measured data and estimating seven parameters (three co-ordinates + four frequencies) in one go. Another possibility is to split the data in four streams, each one corresponding to one of the four frequencies. The emitter co-ordinates and RF for each of the streams are estimated and the co-ordinates are averaged afterwards. This method gives about 5 to 10 % worse results. It is slightly more ill-conditioned (especially for already ill-conditioned scenarios). The probable explanation is the smaller number of measurements available per parameter in this case: $N/4$. For the method used for the table this number is $4N/7 \approx 2N/4$, about twice as large. This leads to a better stability (better CNs). The difference between the two methods is apparently not compensated by the averaging afterwards. The method used for the table is therefore preferred.

8.4.2 X- and y-error as a function of the emitter location

The emitter location error dependence on the emitter distance was discussed in section 6.5, where the average over many random scenarios was taken. In this section we analyse this dependence for a particular setup: the top row of Table 8.2, with the same weaving trajectory, for various emitter locations (x_e, y_e). For this we compute CRLB ellipses as outlined in Chapter 3. For the errors we take the maximum x- or y-values of the CRLB ellipse (not the lengths of the semi-axes).

Figure 8.3 shows the error in the x-direction as a function of the emitter location with the x-co-ordinate between -100 and +100 km and the y-co-ordinate between 0 and +100 km. The negative y-range is omitted because the figure is symmetric with respect to the x-axis. Because the trajectory starts at (0,0) the figure is only nearly symmetric with respect to the y-axis. The base-10 logarithm of the x-error is plotted in the upper plot for clarity's sake. The error mostly increases with increasing distance from the origin. The lower plot gives contours corresponding to the upper plot. The labels in the contours are errors in meters.

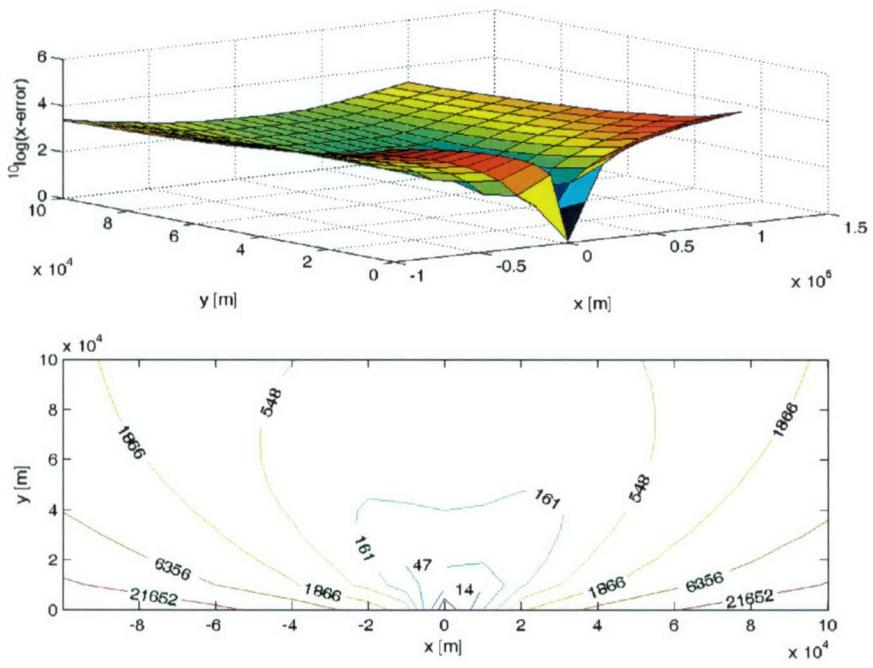

Figure 8.3: x-error. The z-axis of the 3D plot is logarithmic. The labels in the contour plot are errors in meters.

The next figure shows similar plots for the y-error. The conclusions are the same as for the x-error.

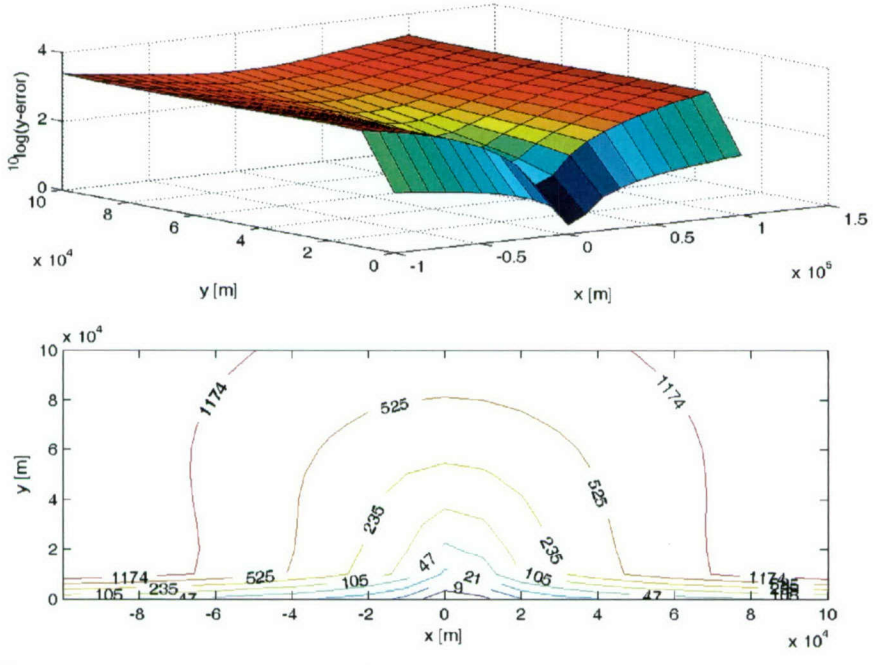

Figure 8.4: y-error. The z-axis of the 3D plot is logarithmic. The labels in the contour plot are errors in meters.

Clearly the accuracy depends on the distance, so absolute accuracy as defined in section 6.5 is not attained. We investigate whether relative accuracy sufficient for a targeting pod with a FOV of 2° is attained. The field of view covers a ground area which is

longer in the range direction than in the cross-range direction. Therefore we restrict the treatment to the more critical cross-range direction.
For this we compute an error angle α for every emitter location. It is defined such that it can be directly compared to the FOV. Details of the computation are in Appendix A. For now we only give a short explanation. Assume a rectangle is drawn centered at the emitter location with the side lengths given by (twice) the appropriate errors from Figure 8.3 and Figure 8.4. For all four corners the (smallest) angle between the slant range plane and the line connecting the aircraft and the corner is computed. The error angle α is now the maximum of the absolute values of these four angles. It can be directly compared to the FOV. Figure 8.5 shows the error angle as a function of the emitter location.

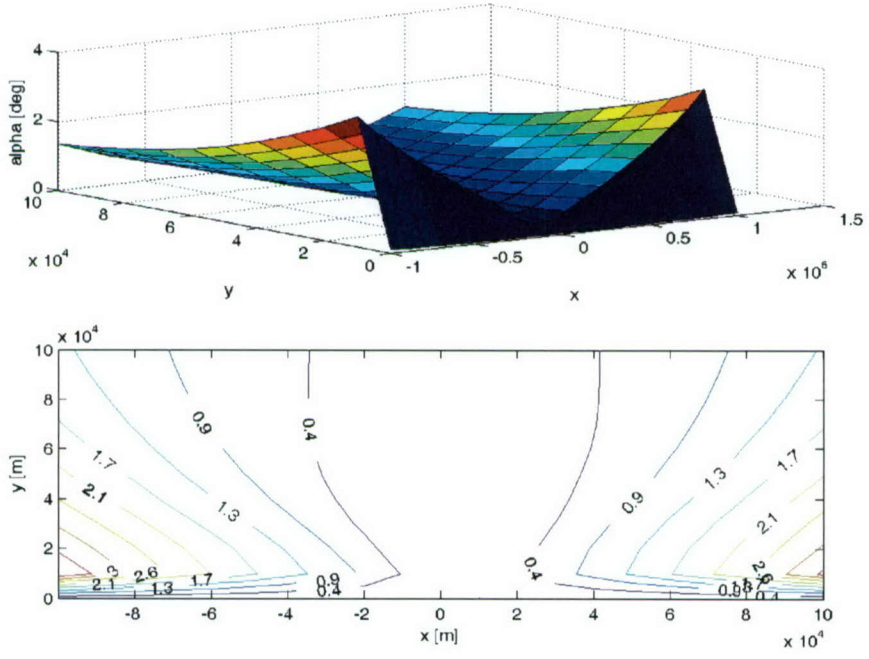

Figure 8.5: Error angle α in a 3D plot (top) with contours (bottom).

For a FOV of 2° the error angle should be below 1°. The plots show that the algorithm is not accurate enough (i.e., does not provide sufficient relative accuracy) over the full area covered by the plot. It does if the FOV is increased to approximately 4°.

8.5 Straight trajectory computations

To our surprise the LSQxyz algorithm did not produce a sensible result for straight-line trajectories. In particular, for a track aligned with the x-axis the CRLB for x was a sensible value, contrary to the values in the y- and z-direction, which tended towards infinity. This can be understood as follows: the Doppler frequency for this particular situation is

$$f_d(t) = -\frac{f_0}{c}\mathbf{v}(t)\cdot\mathbf{u}(t),$$

according to Eq.(2.1). If we assume an aircraft position $(v_a t \quad 0 \quad 0)^T$ and an emitter position $(x_e \quad y_e \quad z_e)^T$ the following simple formula for the Doppler frequency results:

$$f_d = -\frac{f_0}{c} \frac{v_a (v_a t - x_e)}{\sqrt{(v_a t - x_e)^2 + y_e^2 + z_e^2}}.$$

y_e and z_e appear in the same functional form in this formula. As a consequence, given a set of Doppler measurements, the LSQxyz algorithm cannot decide which of the two led to these measurements.

As an example we estimated the emitter location for a sinusoidal trajectory given by

$$\begin{pmatrix} x_a \\ y_a \\ z_a \end{pmatrix} = \begin{pmatrix} 79.8t \\ a \sin(0.2t) \\ 1524 \end{pmatrix}.$$

The smaller the amplitude a the more the trajectory resembles a straight line. Table 8.3 shows the location accuracy for different amplitudes.

Table 8.3: Location accuracy for different amplitudes.

a [m]	bad CN [%]	divergence [%]	x_{50}	y_{50}	z_{50}	f_{50}
1000	0	0	17	8	49	0.9
100	0	0	82	72	168	1.8
10	6	18	115	176	576	2.4
1	44	11	101	1328	2636	2.2
0.1	95	2	114	3599	3638	2.2

The true location of the transmitter is (-5000, -5000) m while the other parameters are those of the top row of Table 8.2. As predicted, the location accuracy in the y- and z-direction degrades with decreasing amplitude, while those in the x-direction and frequency (the average of the four frequency errors) converge. Note also that the algorithm is not even able to find a good solution in many cases for small amplitudes, as indicated by the increasing occurrence of cases with a bad condition number.
When the "bad CN" percentage increases the divergence percentage decreases. Apparently, the "bad CN" condition occurs already before the maximum number of iterations is reached (the condition for divergence). So the algorithm simply quits with a "bad CN" error before it has the opportunity to diverge and quit with a "divergence" error.

Although the previous example involves the special case of a track aligned with the x-axis, it can be generalised to arbitrary track orientations. After all, the emitter is point symmetric (not taking its radiation pattern into account) so the x-axis does not have a special direction. A consequence of a direction non-parallel to the x-axis causes x_{50} to diverge with decreasing amplitude, like y_{50} and z_{50} do.

8.6 Conclusion

A general conclusion is that the LSQxyz algorithm performs worse the more straight a trajectory is, and it cannot handle perfect straight trajectories. LSQxy can handle straight line trajectories, but also benefits from manoeuvring.

9 Conclusions

A (radar or communication) emitter location algorithm utilising frequency (Doppler) measurements done from a single antenna airborne platform was investigated. It estimates the 3D location (x, y, z) of the emitter and its frequency (in reality: a signal down-converted in frequency[5]).

It is proven analytically that the location accuracy benefits in general from small errors in the measured emitter frequency and the measured aircraft velocity. In addition advantageous are a large emitter frequency and a small time interval between consecutive frequency measurements. Errors in the aircraft position measurements are unimportant.

Monte Carlo simulations showed that, if little is known about the measurement scenario, one can assume that the total observation period and the aircraft speed should be both as large as possible. Neither the aircraft altitude nor the emitter altitude is very important.

A three-parameter algorithm variant estimating the 2D location (x, y) and the RF is not accurate enough for operation over The Netherlands. The errors due to the ≈330 m altitude variation exceed those due to the expected frequency accuracy of ≈25 Hz. The three-parameter variant used together with a topographic map functions accurately.

The PESMO test flights are expected to give a location accuracy between ≈30 m (at 5 km range) and ≈30 km (at 200 km range) assuming a 100 s continuous observation period and a 25 Hz frequency measurement error. At least a 25 s observation period is necessary to get a reasonable accuracy. The frequency per burst are averaged by the algorithm used, and it estimates the three co-ordinates and four frequencies in a single run. This algorithm gave the best results of a few variants tested. The algorithm does not provide a range independent accuracy, but it is nevertheless accurate enough to guide a targeting pod with a FOV of 2° over an area of tens of kilometres.

The algorithm estimating the 3D emitter position (LSQxyz) cannot estimate the location if the aircraft followed a perfect straight track. Large errors remain for near-straight tracks. Manoeuvring is therefore of importance. LSQxy handles straight tracks well, but performs bad for targets at non-zero altitude. We conclude that the performance of both LSQxy and LSQxyz should be tested and compared with forthcoming PESMO data.

It should be finally noted that this research was devoted to a single algorithm. Although this algorithm attains the CRLB, which is a lower bound for the average error that can ever be reached by *any* unbiased location algorithm, a combination of algorithms can have advantages. For example, it is not unthinkable that a combination reaches a certain accuracy with fewer measurements than a single algorithm. If needed, this can be investigated in the future.

---

[5] In practice the signal RF frequency is mixed down to one at an intermediate frequency (IF). This lower frequency signal is what is measured. This was not important for the discussion, and we assumed that the RF signal itself was measured.

10 References

[1] F.A.M. Dam, "Emitter location from an airborne platform through precision ESM", TNO report to be published in 2005

[2] M.L. Fowler "Analysis of single-platform passive emitter location with terrain data", IEEE Tr. on AES, Vol, 37, No. 2, April 2001, pp.495-507

[3] M.L. Fowler, "CRLB for radar location via frequency measurements", 2002, www.ws.binghamton.edu/fowler/fowler%20personal%20page/EE522_files/CRLB%20for%20Dopp_Loc%20Notes.pdf

[4] N.E. Wu ad M.L. Fowler, "Application of MEMS for improved emitter location accuracy", Proc. 1st IEEE Conf. on Sensors, Orlando, Florida, June 12-14 2002, pp. 843-848

[5] B.C.B. Vermeulen, R.M.E.M. van Heijster and K.D. Liem, "Precisie ESM ontvanger technologie – Test plan", 2004

[6] A. Theil, "Frequency estimation in ESM systems for emitter location", TNO report to be published in 2005

11 Abbreviations

ASR	Airport Surveillance Radar
CN	Condition Number
CRLB	Cramér-Rao Lower Bound
ESM	Electronic warfare Support Measures
FIM	Fisher Information Matrix
FOV	Field Of View
LSQxy	Least-Squares Algorithm that estimates a 2D location (x, y)
LSQxyz	Least-Squares Algorithm that estimates a 3D location (x, y, z)
PESMO	Precision ESM Receiver technology
PRF	Pulse Repetition Frequency
PSR	Primary Surveillance Radar
RF	Radio Frequency
TNO	Netherlands Organisation for Applied Scientific Research

12 Signature

The Hague

TNO Defence, Security and Safety

Ir. J.P. Dezaire
Group leader

Drs. J.S. Groot
Author

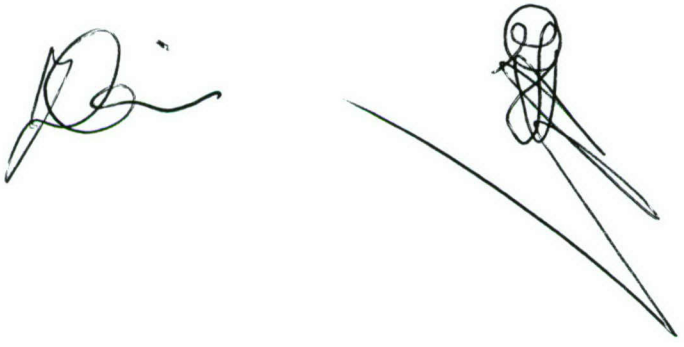

A Computation of the error angle α

Figure A.1 shows the geometry we use to compute the error angle. Numbers between [ ] are the figures used for this drawing.

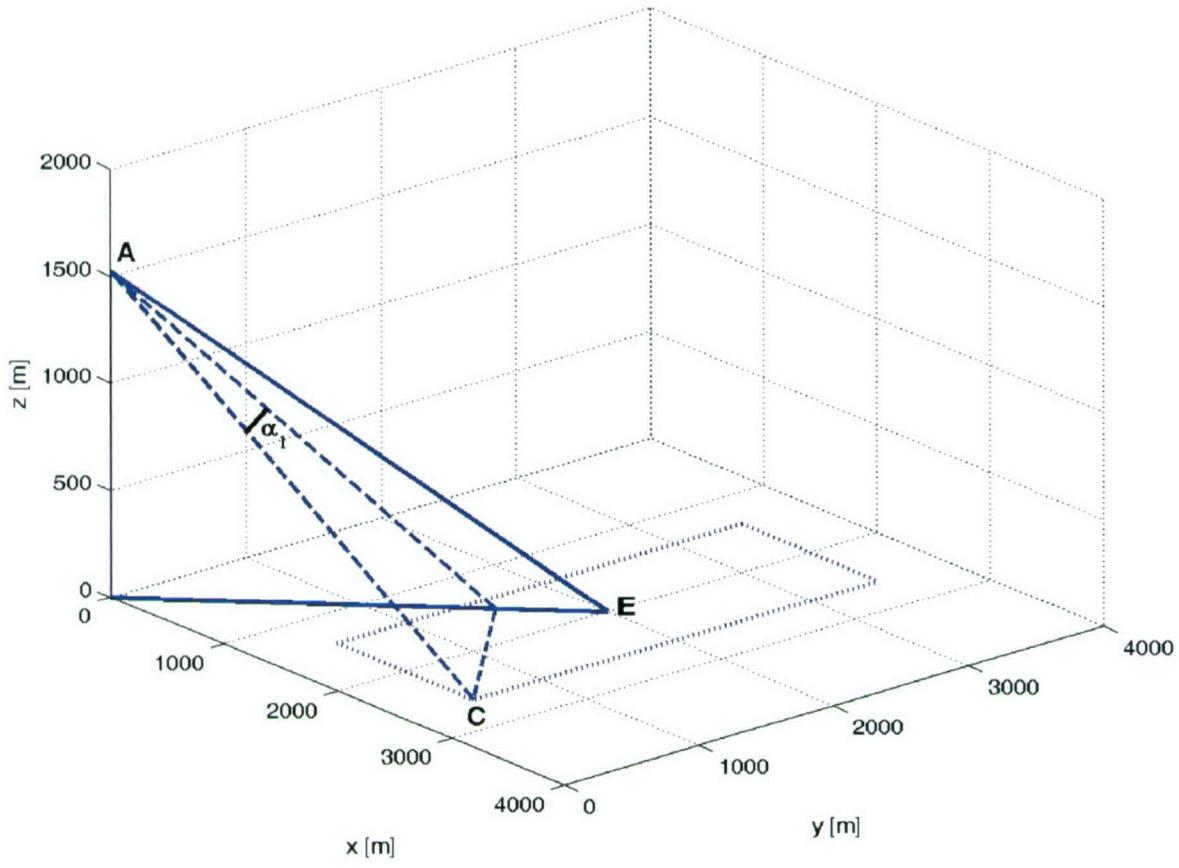

Figure A.1: Geometry of the problem.

Point A= (0, 0, z_a) [0, 0, 1524] is the aircraft position. The emitter is at location E= (x_e, y_e, 0) [2000, 2000, 0]. The rectangle is defined by an error dx [600] in the x-direction and dy [1500] in the y-direction (the errors are greatly exaggerated to make this a clear example). C= (x_e+dx, y_e-dy) is one of the rectangle corners. The angle α_1 is the (smallest) angle between the line AC and plane AEO, with O= (0, 0, 0) the origin. In the same way α_2, α_3, and α_4 are defined for the remaining rectangle corners. The error angle α is the maximum of the absolute value of the four angles. It is this angle that should be compared to FOV/2 to determine whether the algorithm error is smaller than FOV/2. Note that the errors dx and dy are not upper bounds. In reality larger errors (location estimates outside the rectangle) can occur, due to the statistical nature of the problem.

The problem of finding α_1 is solved with vector analysis. We define three vectors:

$\mathbf{a} = (x_e \quad y_e \quad -z_a)^T$ from the aircraft to the emitter .

$\mathbf{b} = (x_e + dx \quad y_e - dy \quad -z_a)^T$ from the aircraft to the rectangle corner.

$\mathbf{c} = (0 \quad 0 \quad -z_a)^T$ from the aircraft to the origin.

A vector normal to the plane AEO plane is given by the cross-product of $\mathbf{a}$ and $\mathbf{c}$:

$\mathbf{d} = \mathbf{a} \times \mathbf{c}$.

The angle α_1 follows from the dot-product of $\mathbf{b}$ and $\mathbf{d}$:

$$\alpha_1 = \frac{\pi}{2} - \arccos\left(\frac{\mathbf{b} \cdot \mathbf{d}}{|\mathbf{b}||\mathbf{d}|}\right).$$

REPORT DOCUMENTATION PAGE
(MOD-NL)

1. DEFENCE REPORT NO (MOD-NL)	2. RECIPIENT'S ACCESSION NO	3. PERFORMING ORGANIZATION REPORT NO
TD2005-0287	-	TNO-DV1 2005 A004
4. PROJECT/TASK/WORK UNIT NO	**5. CONTRACT NO**	**6. REPORT DATE**
015.34097	-	September 2005
7. NUMBER OF PAGES	**8. NUMBER OF REFERENCES**	**9. TYPE OF REPORT AND DATES COVERED**
44 (incl 1 appendix, excl RDP & distribution list)	6	Final

10. TITLE AND SUBTITLE

Analysis of an emitter location algorithm for use in ESM systems

11. AUTHOR(S)

Drs. J.S. Groot

12. PERFORMING ORGANIZATION NAME(S) AND ADDRESS(ES)

TNO Defence, Security and Safety, Location The Hague , P.O. Box 96864 , 2509 JG The Hague , The Netherlands
Oude Waalsdorperweg 63, The Hague, The Netherlands

13. SPONSORING AGENCY NAME(S) AND ADDRESS(ES)

CTL/AJO/HSEOV

14. SUPPLEMENTARY NOTES

The classification designation Ongerubriceerd is equivalent to Unclassified, Stg. Confidentieel is equivalent to Confidential and Stg. Geheim is equivalent to Secret..

15. ABSTRACT (MAXIMUM 200 WORDS (1044 BYTE))

The report analyses a least squares algorithm for 3D emitter location. The data used is a time series of frequency measurements performed by an airborne receiver, in conjunction with speed and position measurements of the platform. The analysis is done analytically as well as through Monte Carlo simulation.

The accuracy generally improves with decreasing frequency and speed errors. A larger RF and a frequent frequency measurement are also beneficial, as are a high aircraft speed and a long observation time. The aircraft altitude is of little importance.

A 2D algorithm variant is too inaccurate in case of 330 m emitter altitude uncertainty.

Simulation of future measurements of an ASR gives an accuracy of 30 m at 5 km range and 30 km at 200 km range, for an observation time of 100 s. The accuracy is sufficient to guide a targeting pod with a FOV of 2 degrees.

16. DESCRIPTORS	IDENTIFIERS
ESM	
Emitter location	
Least squares estimation	

17a.SECURITY CLASSIFICATION (OF REPORT)	17b.SECURITY CLASSIFICATION (OF PAGE)	17c.SECURITY CLASSIFICATION (OF ABSTRACT)
Ongerubriceerd	Ongerubriceerd	Ongerubriceerd

18. DISTRIBUTION AVAILABILITY STATEMENT	17d.SECURITY CLASSIFICATION (OF TITLES
Unlimited Distribution	Ongerubriceerd

Distributionlist

Distributie rapport

1. SC-WOO
2. HWO- KLu
3. KLu/AJO/HSEOV, t.a.v. LtKol J.P. Strijker
4. TNO Defensie en Veiligheid, Directeur Kennis, daarna reserve
5. Bibliotheek KMA
6. Bibliotheek KMA
7. Bibliotheek KMA
8. Archief TNO Defensie en Veiligheid, in bruikleen aan Dr.ir. H.M.A. Schleijpen
9. Archief TNO Defensie en Veiligheid, in bruikleen aan Drs. J.S. Groot
10. Archief TNO Defensie en Veiligheid, in bruikleen aan Ir. F.A.M. Dam
11. Archief TNO Defensie en Veiligheid, in bruikleen aan Ir. A. Theil
12. Documentatie TNO Defensie en Veiligheid
13. Reserve

Distributie managementuittreksel & distributielijst

1× TNO Defensie en Veiligheid, Algemeen directeur,
TNO Defensie en Veiligheid, Directeur Operaties,
TNO Defensie en Veiligheid, Manager Markt,
MIVD / AAR / HBMT

4× SC-WOO, Hoofdcluster Kennistransfer, Kol. A.P. Coppens